Journal of Physics:
Condensed Matter

TOPICAL REVIEW • OPEN ACCESS

Metastable grain boundaries: the roles of structural and chemical disorders in their energetics, non-equilibrium kinetic evolution, and mechanical behaviors

To cite this article: Miao He *et al* 2024 *J. Phys.: Condens. Matter* **36** 343001

OPEN ACCESS
IOP Publishing
Journal of Physics: Condensed Matter
J. Phys.: Condens. Matter **36** (2024) 343001 (21pp)
https://doi.org/10.1088/1361-648X/ad4aab

Topical Review

Metastable grain boundaries: the roles of structural and chemical disorders in their energetics, non-equilibrium kinetic evolution, and mechanical behaviors

Miao He*, Yuchu Wang and Yue Fan*

Department of Mechanical Engineering, University of Michigan, Ann Arbor, MI 48109, United States of America

E-mail: hemiao@umich.edu and fanyue@umich.edu

Received 21 January 2024, revised 9 April 2024
Accepted for publication 13 May 2024
Published 24 May 2024

Abstract

Complex environments in advanced manufacturing usually involve ultrafast laser or ion irradiation which leads to rapid heating and cooling and drives grain boundaries (GBs) to non-equilibrium states, featuring distinct energetics and kinetic behaviors compared to conventional equilibrium or near-equilibrium GBs. In this topical review, we provide an overview of both recent experimental and computational studies on metastable GBs, i.e. their energetics, kinetic behaviors, and mechanical properties. In contrast to GBs at thermodynamic equilibrium, the inherent structure energy of metastable GBs exhibits a spectrum instead of single value for a particular misorientation, due to the existence of microstructural and chemical disorder. The potential energy landscape governs the energetic and kinetic behaviors of metastable GBs, including the ageing/rejuvenating mechanism and activation barrier distributions. The unique energetics and structural disorder of metastable GBs lead to unique mechanical properties and tunability of interface-rich nanocrystalline materials. We also discuss that, in addition to structural disorder, chemical complexity in multi-components alloys could also drive the GBs away from their ground states and, subsequently, significantly impact on the GBs-mediated deformation. And under some extreme conditions such as irradiation, structural disorders and chemical complexity may simultaneously present at interfaces, further enriching of metastability of GBs and their physical and mechanical behaviors. Finally, we discuss the machine learning techniques, which have been increasingly employed to predict and understand the complex behaviors of metastable GBs in recent years. We highlight the potential of data-driven approaches to revolutionize the study of disorder systems by efficiently extracting the relationship between structural features and material properties. We hope this topical review

* Authors to whom any correspondence should be addressed.

paper could shed light and stimulate the development of new GBs engineering strategies that allow more flexibility and tunability for the design of nano-structured materials.

Keywords: grain boundaries, non-equilibrium, mechanical properties, chemical disorder

1. Introduction

The important role of grain boundaries (GBs) in determining materials' properties has received wide consensus from the community [1–4]. In particular, when the grain sizes reduce to nano-meter scale, the high concentration of GBs has been identified as the key contributor to the remarkable mechanical properties observed in nanocrystalline materials. These materials exhibit promising characteristics such as high strength [5–7], enhanced resistance to wear/fatigue [8], and high ductility [9]. In the field of GB-engineering, efforts have been dedicated to manipulating the structure and relative fraction of certain GBs (e.g. twin boundaries or some special low-$\sum$ boundaries) by means of thermo-chemo-mechanical processing to achieve desired materials behaviors [9, 10]. In the past, the majority of investigations were focused on the structures and properties of GBs at or near thermodynamic equilibrium. In other words, for a given misorientation between neighboring grains described by five macroscopic angular degrees of freedom, the primary focuses had been placed on finding the microscopic configuration with the lowest energy state under such macroscopic misorientation angle. As a result, the atomic structures of GBs are often characterized by high coherency and distinguishing structural units [11, 12], such as kites [13–15] and misfit dislocation arrays [16, 17].

Nevertheless, it has been demonstrated more recently by Han and Srolovitz [18], that even under the constraint of a fixed macroscopic misorientation angle there could present broadly and continuously distributed microscopic metastable states with diverse energies and atomic configurations. This indicates the GB structures described above in conventional wisdom would be too 'ideal' when confronted with realistic conditions—in particular the non-equilibrium conditions accompanied with advanced manufacturing and/or processing techniques. For instance, in ultrafast laser-processing or additive manufacturing (AM), materials experience rapid heating and cooling at rates up to 10^{11}–10^{12} K s^{-1} [19–21]. The extrinsic timescale imposed by such swift heating and cooling is much shorter than the intrinsic timescale required for GBs to relax towards their thermodynamic equilibrium, which is mediated by atomic reconfigurations, thus bringing the GBs into non-equilibrium metastable states. The existence of essentially infinite number of metastable microscopic states at the same macroscopic misorientation angle presents new opportunities to engineer and harness the properties of nanocrystalline materials by tuning only the microscopic degrees of freedom without altering samples' macroscopic textures. As an example, femtosecond laser irradiation has been discovered to induce substantial variations (up to 87%) in hardness in nanocrystals, despite negligible alterations in grain sizes [22]. In addition, recent experiments in AM underscore the capacity of non-equilibrium GBs to attain high diffusivity without discernible changes in grain sizes and orientations [23]. These recent progresses collectively envisage a new GB-engineering route—one that focuses on playing with metastability of non-equilibrium microstates while preserving the macroscopic misorientation angles—to complement the conventional GB-engineering strategy and hence to allow more flexibility and tunability for the design of interface-rich nanomaterials.

In this topical review, we aim to establish the fundamental understanding of the unique behaviors and tunability of metastable GBs. We not only discuss the computational studies, but also support the theoretical discoveries by introducing experimental works. In real experiments, AM and laser/ion irradiation are two widely adopted processing techniques to create non-equilibrium environments and thus produce metastable GBs. The contents of this review are organized as the followings: In section 2, we provide an overview of the energetic and kinetic behaviors of metastable GBs, highlighting their distinctions from equilibrium GBs; In section 3, we elucidate how the energetics and kinetics of metastable GBs influence the materials properties (e.g. hardness) in advanced manufacturing; Then, we discuss chemical complexity at metastable GBs and its impact on materials behaviors under mechanical loading (section 4) and irradiation (section 5); Finally, in section 6, we briefly overview the application of emerging techniques, such as machine learning (ML) algorithms, on the prediction of metastable GBs.

2. Kinetics and energetics of metastable GBs

In contrast to idealized equilibrium GBs, metastable GB energies feature large multiplicity due to microscopic degrees of freedom. The existence of metastable GBs results in an energy spectrum in lieu of a single value for a particular misorientation [18, 24, 25]. By adjusting several variables, including the relative translation of grain, placement of the boundary interface, allowed proximity of atoms before one is selected for deletion, and procedures for deleting overlapping atoms, Homer *et al* have sampled over 43 million GB structures from 7304 minimum energy GB structures in Al [26]. The GB energies as a function of disorientation angle for the full set of GB structures including a variety of metastable GBs are illustrated in figure 1(a). The dense spectrum of metastable states where GBs can be locally trapped is analogous to that of glasses, indicating that metastable GBs exhibit glass-like behaviors [27]. In glassy materials, the local minima in a system's underlying potential energy landscape (PEL) are recognized as the inherent structure (IS) energy [28–30]. The kinetic behaviors of the materials are governed by the progressive

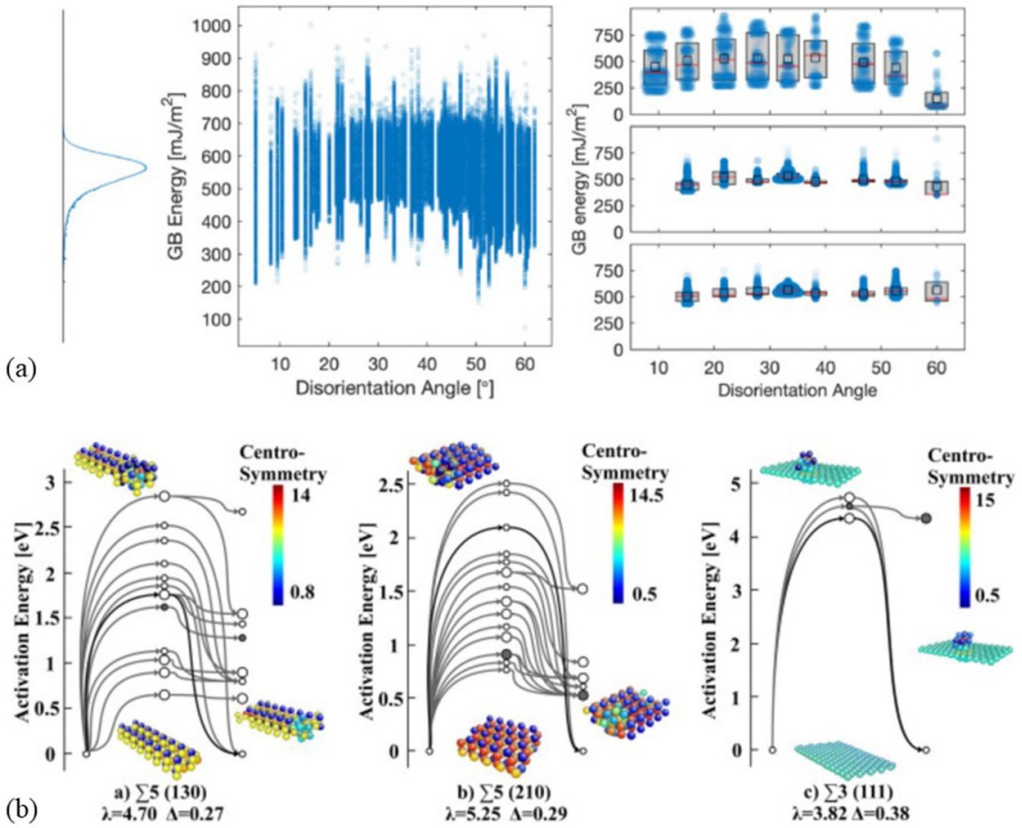

Figure 1. (a) Plots showing the energy of a variety of stable and metastable GB structures (left) and the structures for the [111] twist and symmetric tilt GBs (right). Reprinted from [26], Copyright (2022), with permission from Elsevier. (b) Energy landscape for three series of grain boundaries in Cu. The nodes correspond to accessible GB states and those with similar energy are shown as a single large node. The atomic configurations corresponding to the shaded nodes are shown nearby, where atoms belong to FCC are blanked. Reprinted from [33], Copyright (2013), with permission.

exploration of various ISs in the PEL, more specifically, by a series of energy basins (representing stable and metastable GB states) and the shape of interconnecting pathways between them. Similar to amorphous glassy materials, the ISs analyses have also been employed to study the structure-property relationships in GBs [31]. By implementing the activation-relaxation technique (ART) [32], Alexander and Schuh [33] have built the PEL for three series of GBs in Cu. As shown in figure 1(b), the energies of accessible states including minima and transitional states are plotted. The complexity of metastable GBs is revealed by the multiplicity of local energy minima and disordered atomic structure.

The first implication from the PEL of metastable GBs is an intriguing ageing/rejuvenating mechanisms discovered by Bai *et al* [34]. In their computational study, a multiplicity of metastable microstates under the same macroscopic misorientation constraint (e.g. <100> symmetric tilted bi-crystal) were generated, followed by atomistic simulations of isothermal annealing at a series of temperatures. The IS were obtained through energy minimization of the atomic configurations at 0 K. The evolution of IS energy with time, and subsequently their time derivatives, $(\partial E_{\mathrm{IS}}/\partial t)\,|_T$, were calculated and mapped in figure 2(a), showing the existence of two regimes colored in blue and red, respectively. The blue one is called ageing regime, featuring the decrease of E_{IS} to a lower level, and the red one depicts a rejuvenating regime characterized by an increase in E_{IS}. These findings indicate the metastable GBs' evolution under thermal fluctuation not only is dependent on the environment temperature, but also exhibits strong sensitivity to the metastability level of the sample. This ageing/rejuvenating mechanism is related to sequential transitions in the systems' PEL, resulting from the energy imbalance between uphill climbing and downhill dropping. Similar phenomenon has been reported in metallic glasses [28].

The metastable GBs in figure 2(a) were created by random perturbation of a Σ5 (310) symmetric tilt grain boundary (STGB). In reality, GBs can be driven away from equilibrium and trapped at various metastable states in the course of rapid heating and cooling, i.e. in AM. As manifested in figures 2(b) and (c), Bai *et al* applied fast heating and cooling cycles to the ground-state Σ5 (310) STGB, and observed hysteresis behaviors where the GB energy during cooling lies above the heating curve. Figure 2(c) demonstrates that the magnitude of the hysteresis increases with the heating/cooling rate, due to the inability of the system to relax in a short period of time. Intriguingly, anomalous behaviors emerge when the thermal cycle is interrupted, followed by cooling from intermediate temperatures. As manifested in figure 2(b), cooling from

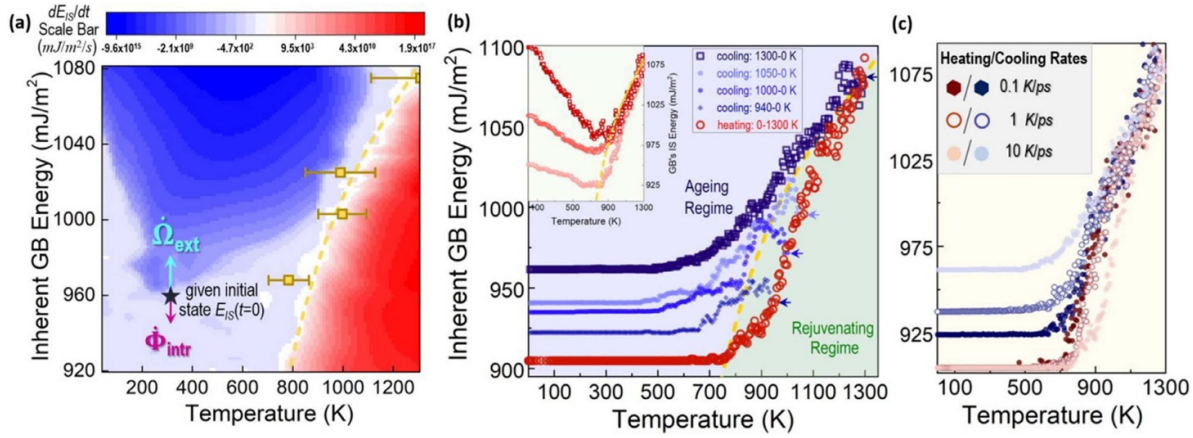

Figure 2. (a) Resolved pixel map illustrating the ageing and rejuvenating behaviors of a series of metastable GBs in Cu. The time derivate of GB's IS energy are predicted from atomistic simulations at a broad range of IS energy, E_{IS}, and temperature, T. The red and blue regimes correspond to rejuvenating $(\partial E_{IS}/\partial t)|_T > 0$ and ageing $(\partial E_{IS}/\partial t)|_T < 0$ behaviors, respectively. The dashed yellow curve represents the boundary separating the ageing and rejuvenating regimes. (b) The evolution of GB's during the heating and cooling cycles with 10 K s^{-1}. The dashed yellow line is the ageing/rejuvenating crossover boundary in (a). (c) The GB energy evolution at different heating/cooling rates. Reprinted from [34], Copyright (2020), with permission from Elsevier.

940, 1000, and 1050 K leads to an initial increase in energy before subsequent decreases, forming a peak which coincides with the ageing-rejuvenating boundary. Notably, these peaks align well with the ageing/rejuvenating crossover boundary in figure 2(a), affirming the universality of the ageing and rejuvenating mechanisms across various external stimuli.

Another implication from the PEL of metastable GBs is the kinetics of GB migration. Previous studies have discovered that GB migration is dependent on the microscopic degrees of freedom and proceeds through transitions between the stable and metastable GB structures [35, 36]. Abrupt change in the activation energy of GB self-diffusion has been reported at elevated temperature, and attributed to phase transition of GB into highly disordered states [14, 37]. Bai *et al* [38] calculated the activation barriers through atomistic simulations based on the IS energy landscape during the rapid heating/cooling cycle. Their computational results revealed a broad spectrum of activation barriers which, as illustrated in figure 3(a), varies significantly at different stages of the heating/cooling cycle. Especially, lower effective activation barriers were observed for high-energy metastable GBs compared to their relaxed, low-energy counterparts. This phenomenon can be explained by the emergence of easily accessible activation pathways facilitated by more random and disordered states of high-energy metastable GBs. Similar effects of metastability on GB kinetics have been revealed that GBs with lower coordination number show smaller activation energies than more ordered boundaries with large coordination number [39].

In figure 3(b), Bai *et al* shows the free volume distribution at different stages of the heating/cooling cycle, calculated as the ratio of Voronoi volumes between non-FCC and FCC atoms. The free volumes during rapid heating and cooling exhibit much broader distribution compared to the initial state (ground-state GB), due to more disordered configurations of metastable GBs. However, as indicated by the vertical lines in figure 3(b), the variance of average volume ratios at different stages of the heating/cooling cycle remains negligible, despite of significant change in the activation energy spectra, figure 3(a). Prior investigations into ground-state GBs with varying misorientation angles have established a positive correlation between their energies and excess free volumes [12, 40]. However, the results in figures 3(a) and (b) imply that conventional belief of volume-mediated diffusion in GBs [41, 42] does not hold for metastable states. This observation suggests that the GBs' metastability is propelled by disorder rather than free volume, which aligns with recent studies on ion irradiated ceramic nanocrystals [43]. In fact, Bai *et al* have demonstrated that in contrast to low-energy metastable GBs (e.g. H-1000 K), more disordered, high-energy GBs (e.g. C-1000 K) features a rougher energy landscape with higher fraction of easily accessible and low-barrier pathways, resulting in facilitated atomic diffusion that cannot be explained by the difference in free volume. This energy landscape-driven instead of free volume-driven mechanism corroborates with the findings in the excitations in metallic glasses [30, 44].

The special kinetic characteristics of metastable GBs explain experimental observations of GB diffusion. Choi *et al* [23] measured isotope diffusion in additively manufactured high-entropy CoCrFeMnNi alloy. The AM process involving laser melting brought the alloy under recurrent, rapid heating/cooling conditions, resulting in the formation of various high-energy metastable GBs, figure 3(c). Ni isotopes were used to measure the diffusion under annealing at 500 K, which is called diffusion annealing. GB diffusion was examined by measuring the radioactivity of the Ni tracer penetrating into the specimen. The penetration profile in the as-prepared AM specimen B is plotted in figure 3(c), along with two benchmark profiles from samples without diffusion annealing and with a pre-annealing at 773 K, respectively. The as-prepared AM sample displays significantly deeper tracer penetration, in stark contrast to the other two cases, where the radioactivity drops rapidly with no tracer atoms detectable beyond a depth

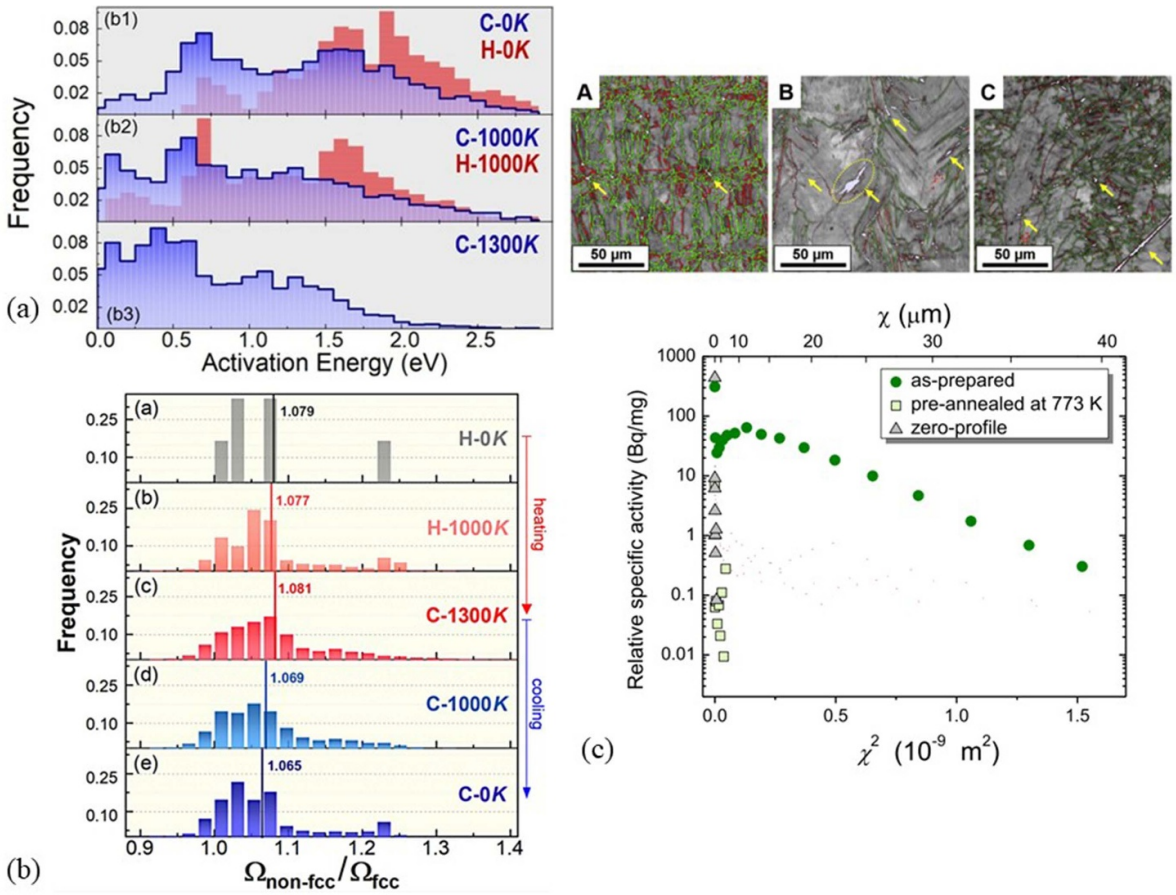

Figure 3. (a) Activation energy spectra and (b) distributions of the ratio of Voronoi volumes between non-FCC and FCC atoms for stable and metastable GBs at different stages of the rapid heating/cooling cycle from a Σ5 (310) STGB in Cu. Reproduced from [38]. CC BY 4.0. (c) (upper panel) SEM images of grain boundaries in three AM samples. High- and low-angle GBs are represented by green and red lines, respectively. (lower panel) Penetration profiles of Ni tracer in specimen B (green circles), specimen without diffusion annealing (triangles up), and specimen pre-annealed at 773 K (squares). Reprinted from [23], Copyright (2020), with permission from Elsevier.

of 3 μm. The remarkable enhancement of tracer diffusion in AM specimen is related to AM-induced non-equilibrium GBs, which are relaxed during pre-annealing. Based on the penetration profile of AM-prepared sample, the diffusion coefficients were estimated to be on the order of 10^{-16} m^2 s^{-1} . Compared to typical values in the well-annealed cast counterparts [45], AM-induced non-equilibrium GBs lead to approximately 10^4–10^8 orders of magnitude increase in GB diffusion. Such boost of GB diffusion in metastable GBs quantitatively aligns with the estimations by Bai *et al* based on computational calculations of activation barriers [38].

Recently studies also show abnormal migration behaviors for metastable GBs. For example, Homer *et al* have found that the existence of low activation barriers may lead to the non-Arrhenius behavior where GBs migrate faster at low temperatures [46]. As shown in figure 4, as the intrinsic barrier height Q drops, the GB velocity dependence on temperature changes from Arrhenius to anti-thermal behaviors. At high barrier of $Q = 1.05$ eV, the migration is only activated at high temperatures. At intermediate barrier of $Q = 0.09$ eV, the GB velocity is detectable at low temperatures, followed by a prolonged region of plateau. When the barrier is extremely low, $Q < 0.03$ eV, the GB velocity shows an inverse, non-Arrhenius dependence on temperature. This can be explained that with low activation barrier, the forward atomic jumps can be activated at low barriers, while with increasing temperature, the increased frequency of backward jumps slows the overall GB migration.

3. GBs' metastability-modulated properties changes

The evolutions of energetics and kinetics in non-equilibrium metastable GBs differ significantly from those observed at or near equilibrium, imparting crucial implications for the properties of nanocrystalline systems. The effects of local atomic structure and stoichiometry on the tensile strength of metastable GBs have been investigated in SiC [47]. Based on the atomistic simulations of nanocrystalline Cu, Vo *et al* have revealed that under different strain rates, the degree of GB relaxation controls the yield strength [48]. Moreover, they found that the yield strength exhibits an inversely relationship with the GB energy with fixed grain size [49], as shown in figure 5(a). Similar trends have been reported in atomistic simulations of nanocrystalline Ni [50], where enhanced

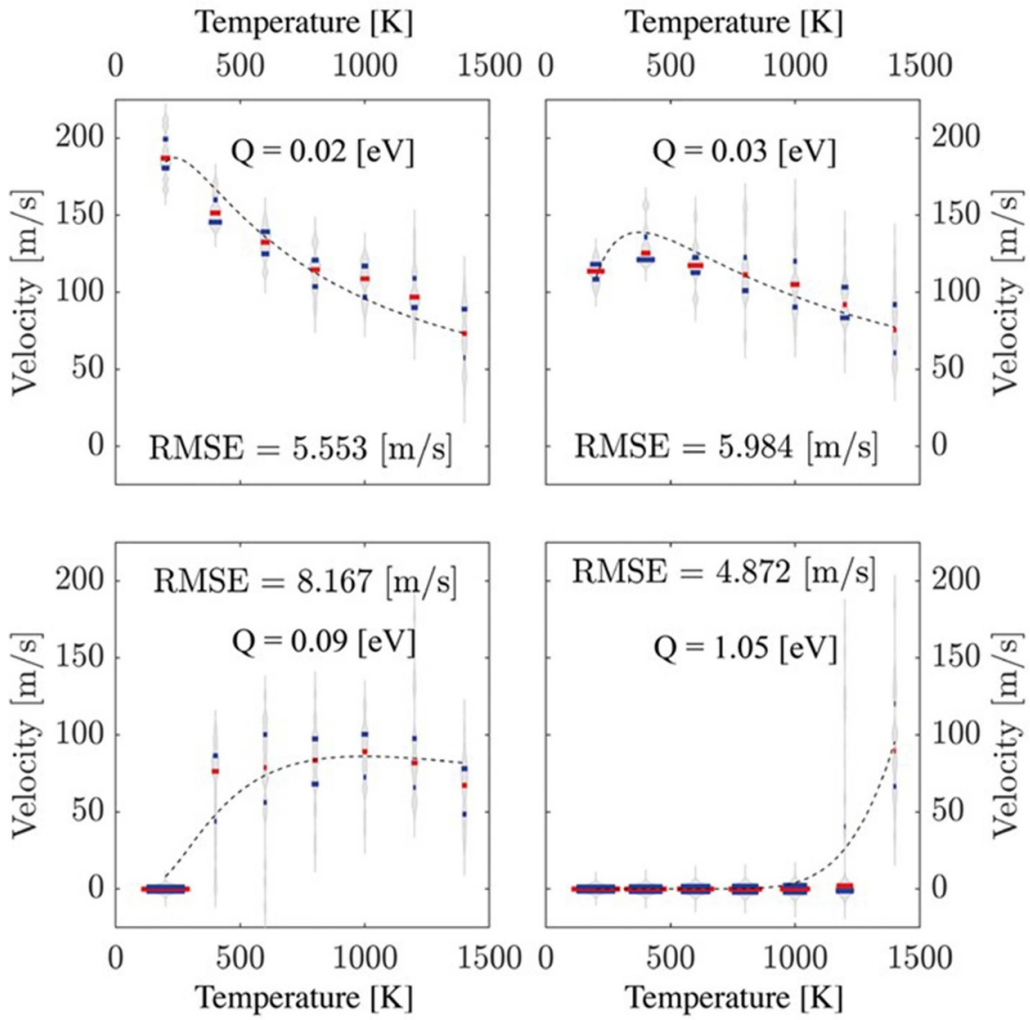

Figure 4. Dependence of GB velocity on temperature for four metastable GB structures with different values of intrinsic barrier Q. Reproduced from [46]. CC BY 4.0.

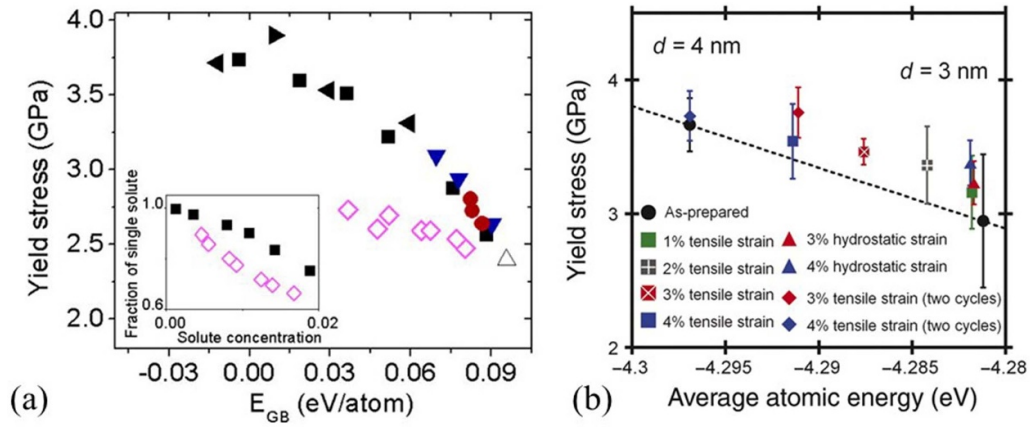

Figure 5. Molecular dynamics predictions of (a) yield stress as a function of GB energy for a series of GBs in Cu alloy. Reprinted from [49], Copyright (2011), with permission from Elsevier and (b) yield stress as a function of average atomic energy for specimen of nanocrystalline Ni under different mechanical treatment. [50] [2011], reprinted by permission of the publisher (Taylor & Francis Ltd, www.tandfonline.com.).

strengths were achieved by relaxation of the non-equilibrium GBs towards lower energy states through cyclic mechanical loading. As indicated from figure 5(b), multiple loading cycles up to larger strains lead to more relaxed GB structures, which are associated with lower average atomic energies, as well as increased yield stresses. In addition, it has been shown that the

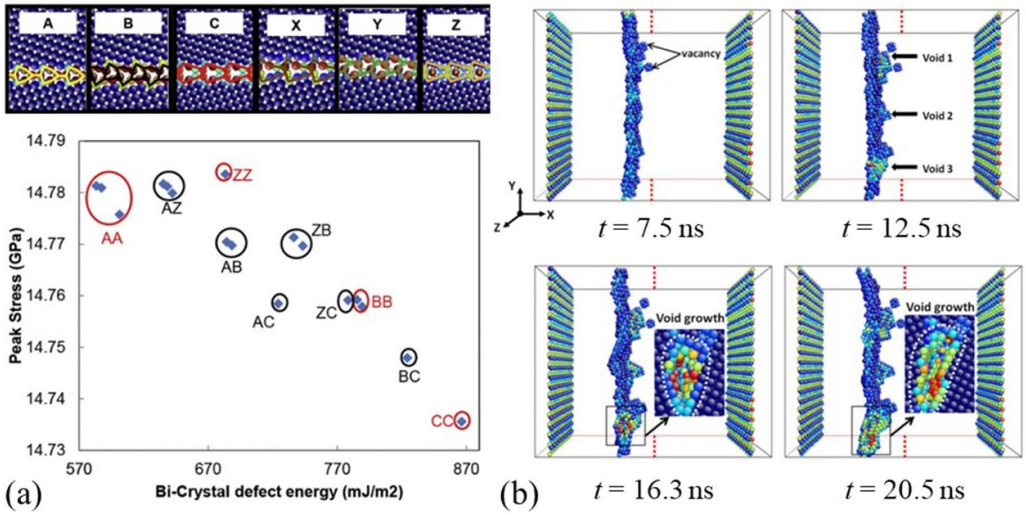

Figure 6. (a) Yield strength depending on energy for bi-crystal Al with different combinations of GB structures. Reprinted from [55], Copyright (2016), with permission from Elsevier. (b) Evolution of a metastable GB structure in a bi-crystal Al under shear deformation at 10 K. Atoms are colored based on the centrosymmetric parameters, and those with fcc structure is blanked except in the enlarged images. Initial GB position is remarked as the red dotted lines. Reproduced from [56]. © IOP Publishing Ltd. All rights reserved.

energetic characteristics of GBs rather than their specific morphologies exert a greater influence on the strength and mobility [51]. Notably, such significant role of inherent energy in nanocrystalline systems have been identified in amorphous materials as well [30, 52–54].

However, in contrast to the simply inverse relationship between the strength and GB energy, Burbery *et al* found intriguing results that some high energy GBs have higher strength than that of lower energy GBs [55]. In their molecular dynamics (MD) simulations, the system was represented by a bi-crystal of Al with periodic boundary conditions containing two GBs. As illustrated in the atomic configurations in figure 6(a), stable (*A*) and metastable (*B, C, X, Y* and *Z*) GB structures were generated, and a series of combinations between these GB structures were investigated. The plot in figure 6(a) shows the athermal strength for different bi-crystal structures as a function of energy. It can be seen that distinct strength is observed for bi-crystals with different GB combinations, despite of identical GB energies. Moreover, compared to the stable minimum energy bi-crystal with '*AA*' GB combination, the bi-crystal with '*ZZ*' GBs has even greater strength. The results indicate that the GB structures, e.g. free volume and centro-symmetry atomic bonding, have significant influence in the mechanical properties. The effect of metastable structures on the mechanical response of GBs is also highlighted by Zhang *et al* [56]. Figure 6(b) manifests the evolution of a metastable GB structure during shear deformation at 10 K. Zhang *et al* found that GB sliding, i.e. translation of one grain over another in the direction parallel to the grain interface, dominates the deformation process. After 12.5 ns, supersaturated vacancies emitted from the GB during GB sliding grow into voids and drag the GB from further motion. As a result, GB sliding becomes the sole deformation mechanism to accommodate the system stress. The GB sliding mechanism is correlated with the uncoordinated movement of inhomogeneous structural units and prominent for disordered metastable GBs, and significantly impacts the mechanical behaviors such as cracking at GB. A review of these previous studies indicates that a profound understanding of the structural-property relationships of metastable GBs enables the control of their microstates and properties in materials, facilitating the optimization of their mechanical performance, which is known as grain boundary engineering.

Grain boundary engineering is particularly important in AM, which typically involves ultra-fast laser irradiation of materials and generation of various metastable through rapid heating and cooling. Balbus *et al* investigated how laser irradiation leads to the variation of mechanical properties, i.e. hardness, in nanocrystalline metals [22]. In figure 7, the dependences of hardness on normalized laser fluence are presented for both the Al-4.8 at.%O and SC–Cu–Zr nanocrystals. With the laser fluence increasing up to the ablation threshold, both samples manifest approximately an ∼80% maximum reduction in hardness. The reduction in hardness can be recovered through relaxation annealing, i.e. at an undercooling level of 0.51. This phenomenon is explicable by the laser-induced rapid heating and subsequent cooling, causing GBs to deviate from the equilibrium state with elevated energy, figures 2(b) and (c). Subsequent annealing facilitates the recovery of metastable GBs towards the initial low-energy state. Bai *et al* [34] provided a viable theoretical/numerical approach to predict metastable GBs' energetic evolution and properties changes. With parameters rationalized based on the experimental conditions, they found uphill energy variation with increasing laser fluence. Given the inversely proportional relationship between the hardness and GB energy, such energetic evolution implies an anticipated decrease in the sample's hardness as laser fluence increases, which aligns well with the experimental results in figure 7.

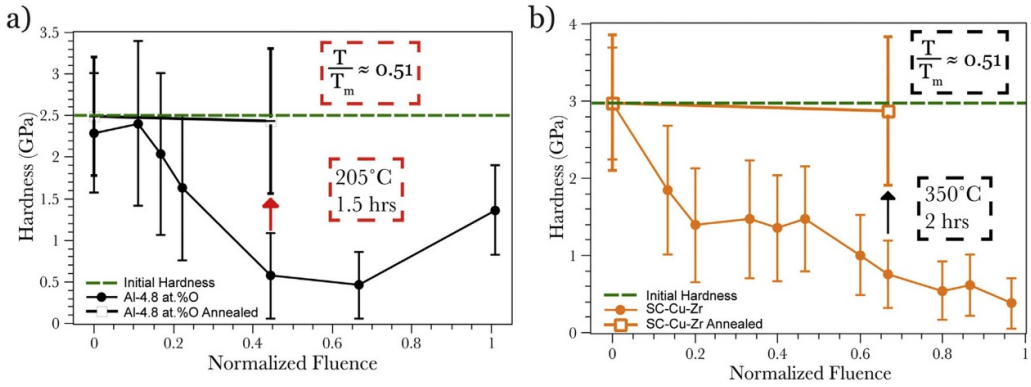

Figure 7. Dependence of hardness on the normalized laser fluence for the (a) Al-4.8 at.%O and (b) SC–Cu–Zr nanocrystalline metals. Filled black circles in (a) and filled orange circles in (b) depict the initial measurements before annealing. Open black squares in (a) and open orange squares in (b) correspond to the measurements after annealing at 205 °C for 1.5 h and at 350 °C for 2 h, respectively. Reprinted from [22], Copyright (2018), with permission from Elsevier.

4. Role of chemical heterogeneity in GBs' deformation behaviors

In addition to the above-discussed structural disorders in metastable GBs, change of the chemical complexities would also lead to different energy states of the GB samples, and the inherent chemical complexities in multi-component alloys further enrich the GB-mediated deformation behaviors. For example, it has been shown that element segregation and local chemical order (LCO) could impact the chemical heterogeneity across the interfaces, which thus affecting how GBs resist dislocation activities and strengthen alloys [57–59]. Through tensile testing simulations, Wu *et al* [60] investigated the effect of LCO, i.e. segregation of Cr at the GBs, on the stability of GBs and dislocation nucleation in nanograined (NG) high-entropy alloys (HEAs), specifically the FeCoNiCrMn HEAs. NG HEAs are studied in this research because materials with a NG structure typically experience reduced thermal stability, a consequence of the significant proportion of GBs. MD simulations were utilized to study NG FeCoNiCrMn HEAs. Their computational results are shown in figure 8(a). When the strain reaches 8%, it was observed that the GBs containing LCO (the second row) exhibited reduced shear strain compared to random GBs (the first row). This suggests that LCO effectively stabilizes the GBs and hinders their movement. At the strain of 16%, less Shockley partial dislocations were observed in the system with Cr segregated GBs compared to that with random GBs, suggesting that the nucleation and movement of dislocations are hindered by LCO at GBs. Similar phenomenon was also demonstrated in the computational study of Li *et al* [61] in a prototypical CoCrFeMnNi HEAs system. In this study, the activation energy of atoms in GBs was calculated through the advanced proactive energy landscape sampling algorithm, activation relaxation technique [62–64]. The activation energy spectra of grain boundary atoms of the samples with 50% Fe- and Cr-segregation at GBs were investigated respectively. As shown in figure 8(b), Fe-segregation at GBs leads to lower yield strength than Cr-segregation, which is attributed to a fast dislocation density increment in the Fe-segregated sample. In Fe-rich GBs, the activation energy spectra suggests that the collective mode (i.e. coordinated atomic displacement such as dislocation emission) not only matches but also surpasses the random mode (i.e. diffusive shuffle of local atoms). This enhancement in the collective mode actively encourages slip activity and the generation of Shockley partial dislocations. It should be noted that, the role of a specific element is not invariant and instead should depend on given samples' global composition. For example, in a previous study on the interactions between GBs and stacking fault tetrahedron (SFT), Li *et al* [65] reported that with increasing Fe concentration, the migrating GBs in Ni–Fe alloys has a higher efficiency to heal the SFT. These findings above demonstrate the complexities and challenges in fully understanding the GB-mediated deformation amid both structural and chemical disorders, but meanwhile also indicate the vast parameters space to tune the samples' mechanical performance.

Wang *et al*'s study [66] highlights the significant role of chemical heterogeneity in the deformation behaviors of GBs when subjected to cyclic mechanical loading. Their primary focus was on understanding crack propagation in Fe–Ni–Cr alloy, a complex process highly sensitive to various influencing factors [67–69]. More specifically, numerous experimental studies have reported a notable phenomenon of non-monotonic changes in ductility—a loss of ductility at intermediate temperature—in the similar alloy system across various compositions, indicating a universal mechanism underpinning. Sun *et al* [70] studied the intermediate-temperature brittleness in a ferritic 17Cr stainless steel. They observed that this brittleness, characterized by a low reduction of area, occurred near temperatures of 810–970 K and found that the brittleness shifted to higher temperatures at higher tensile strain rates. Trelles *et al* [71] revealed that the material DCI GJS-500 exhibited embrittlement at temperatures nearby 400 °C, leading to a significantly higher fatigue crack growth rate and a reduced lifetime. Zheng *et al* [72] discovered that the Ni(Bi) alloy exhibited clear intermediate temperature embrittlement with a minimum ductility observed between 700 °C and 750 °C, unlike the high-purity Ni, which

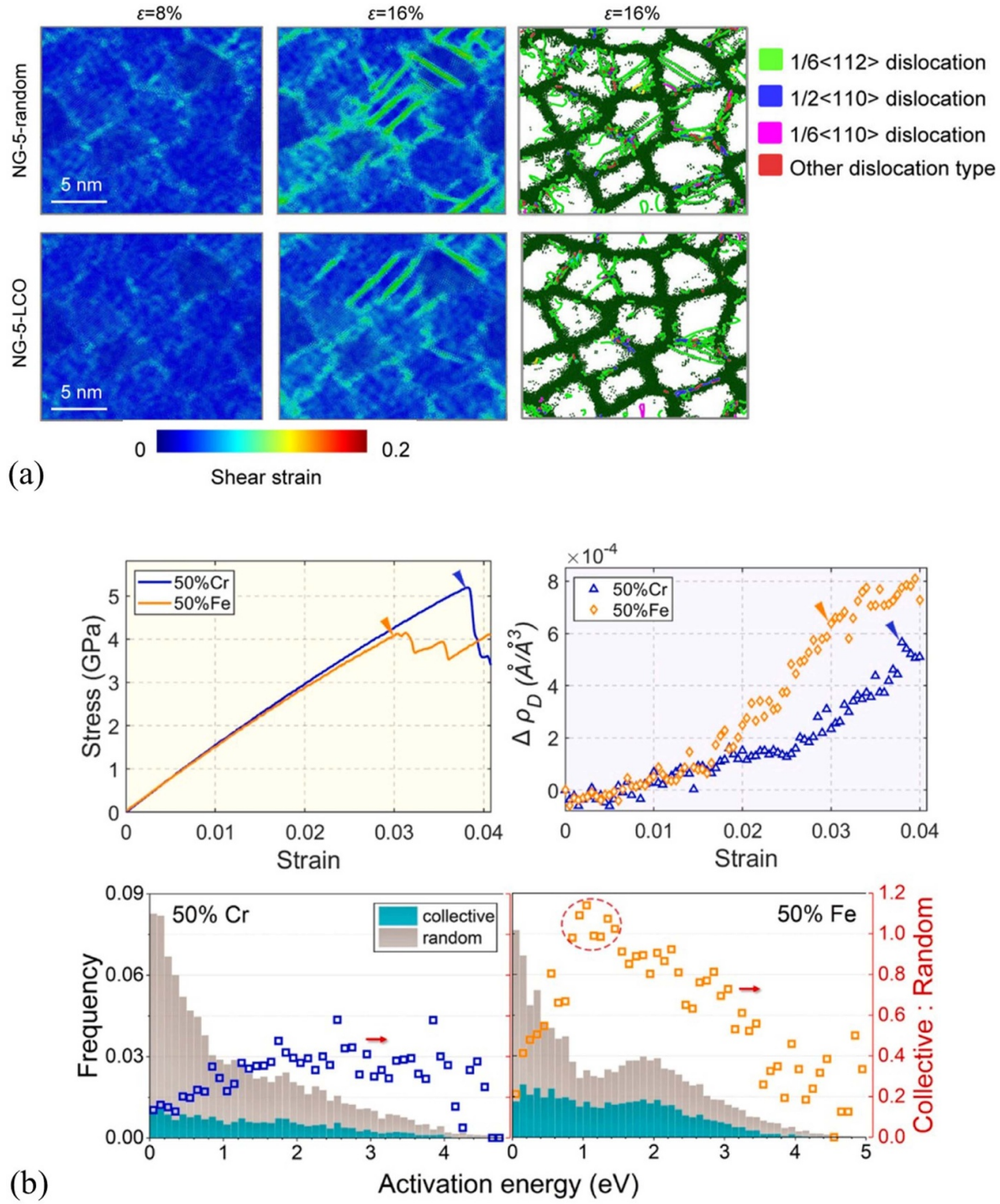

Figure 8. (a) (Left) 200 K, the dislocation arrangements at the strain of 16% and the distribution of shear strain within the NG FeCoNiCrMn HEA during tensile loading. (Right) visual representations of the grain boundary structures. Reproduced from [60], with permission from Springer Nature. (b) Stress strain curve (upper left), dislocation density increment (upper right), and decomposed activation energy spectra by stacking the frequency of random and collective modes (lower panel) for bi-crystalline CoCrFeMnNi HEA sample with 50% Cr and Fe segregation during mechanical loading. Reprinted from [61], Copyright (2023), with permission from Elsevier.

did not demonstrate such embrittlement. Jang *et al* [73], in their research on hot-rolled CrMnFeCoNi HEA, also found a significant decrease in yield strength at intermediate temperature. Ming *et al* [74] investigated the phenomenon of ductility loss at intermediate temperatures in single-phase face-centered cubic structured CrMnFeCoNi HEAs. However, a fundamental explanation for this phenomenon is still lacking. In Wang *et al*'s study, to explore the nonmonotonic ductility, they conducted atomistic simulations using Fe–Ni–Cr alloy while maintaining crystallography, size, and thermomechanical stimuli, the same. Symmetrically tilted grain boundaries (STGBs) were involved in the samples. The Metropolis

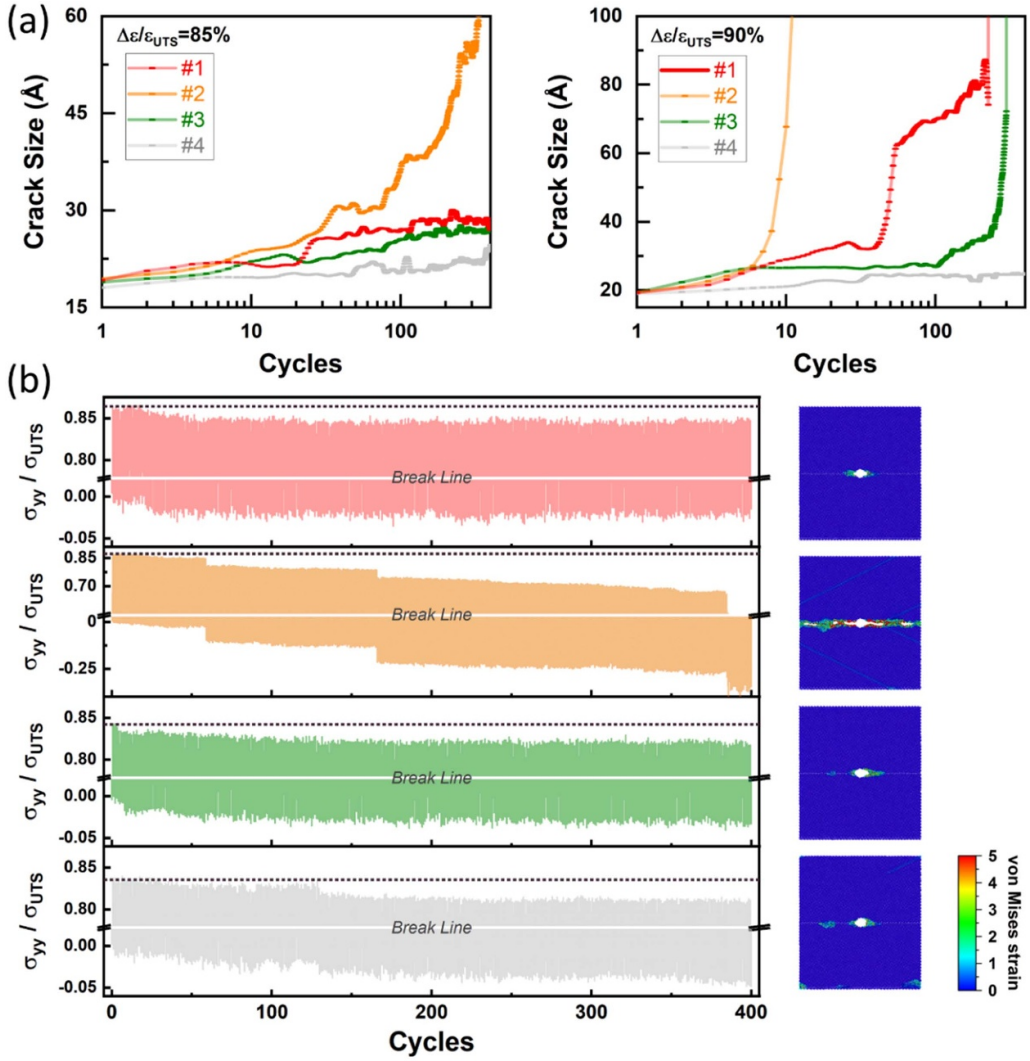

Figure 9. (a) Maximum strain during cyclic loading is (Left) 85%, (Right) 90% of ε_{UTS}. (b) The change of global normal stress and the von Mises strain distributions when maximum strain is 85% of ε_{UTS}. Reprinted (figure) with permission from [66], Copyright (2023) by the American Physical Society.

Monte Carlo (MC) algorithm was employed to get different levels of Cr segregation [75, 76]. With the MC algorithm, they obtained different chemical heterogeneity at high-angle GBs (HAGBs), as well as different energy states. Consequently, the chemical complexity transformed the ground state STGBs into metastable GBs at different energy levels. During the study, a preexisting nanovoid was placed on the GBs and Wang *et al* compared the growth of the crack under cyclic loading conditions. As depicted in figure 9, their findings revealed that crack propagation was fastest in sample #2, corresponding to an intermediate level of chemical heterogeneity within the GBs.

They also examined four HAGB samples with the chemical composition to be $Fe_{70}Ni_{10}Cr_{20}$, denoted as #i to #iv in figure 10(b), each displaying varying levels of Cr segregation, ranging from a completely random solid solution (RSS) to a well-segregated state. Worth noticing, these samples did not exhibit any structural anomalies, such as preexisting cracks. In figure 10(a), each line connects the state before and after the loading cycle, which depicts the decrease of atomic stress after one cycle in red while an increase in blue. While it is difficult for bare eyes to trace each individual curve, such atomic-level stress distributions around the GB particles reveal that the stress fluctuations near the HAGBs exhibit nonaffine characteristics. Notably, in figure 10(b), the intensity of these nonaffine stress fluctuations reaches its peak at an intermediate segregation level of Cr. Such a phenomenon results in a higher frequency of extreme-stressed particles concentrating ahead of crack tips, accelerating the crack propagation.

5. Role of chemical complexity in GB-defects interaction under irradiation

Chemical heterogeneity in GBs attracts great interests in AM, which typically involves irradiation and induces the well-known phenomenon of chemical segregation or LCO. In addition to chemical complexity, laser or ion irradiations also

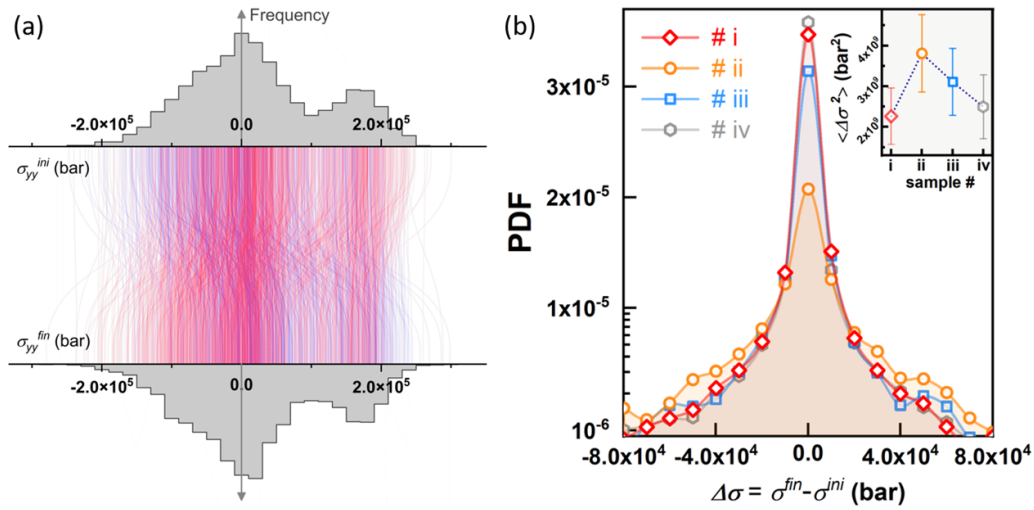

Figure 10. (a) The distribution of probability density (PDF) of atomic stress of the GB atoms in sample #ii (Upper) before and (Lower) after the loading cycle. The change for each atom's stress is depicted in the middle part (red means decrease while blue shows the increase). (b) The PDF of atomic stress changes $\Delta\sigma_i$ in samples #i-#iv. The averaged second moments from 6 samples for the four states are shown in the inset. Reprinted (figure) with permission from [66], Copyright (2023) by the American Physical Society.

produce various defects including point defects, point defect clusters, and dislocations, in the laser-melted region or collision cascades [77–79]. Compared to single crystalline structure, nanocrystalline materials exhibit improved mechanical properties and thermal stability against irradiation [80–84]. Both experimental [80, 85, 86] and computational [87–89] studies have demonstrated the GBs as sinks that effectively absorb the defects and enhance the irradiation resistance. Under electron irradiation, the diffusion of defects towards the GB sinks is believed to be responsible for the suppression of defect clustering, leading to a dislocation-free zone near GB regions [90]. Intriguingly, the sink efficiency of GBs exhibits notable heterogeneity and varies with the energy level, disorientation angle, etc [86, 87, 89, 91]. The evolutions and distributions of point defects in the single-crystalline, bicrystalline, and twinned crystalline copper have been explored by Peng *et al* [92] They found that the interstitials are preferentially segregated near GBs, and the absorption efficiency and influence rage increase with GB energy. Moreover, by comparing the radiation tolerance between equilibrium and non-equilibrium GBs, it is evident that the latter exhibit stronger sink efficiency, resulting in the reduction in both the average size and number of defect clusters, i.e. dislocation loops [93].

The inherent chemical heterogeneities are believed to drive GBs towards spontaneous roughening structure and different energetics [94, 95], resulting in interactions with defects that differ from those observed in single-component systems [96]. From the perspective of GB engineering in advanced manufacturing, understanding of the coupling between the chemical and mechanical behaviors under irradiation facilitates the tailoring of the GB chemical complexity as well as materials properties. An atomistic modeling study of ion irradiation on four types of STGBs in Fe–Cr alloy was carried out by Zhang *et al* [97]. They found that in addition to the preferential absorption interstitials towards GBs, the segregation energy of Fe interstitials is higher than that of Cr interstitials, implying a strong sink efficiency for Fe interstitials. The excess Fe interstitials at GBs have strong interaction with nearby vacancies and may induce annihilation through via the 'interstitial emission' mechanisms [98]. Li *et al* [99] explored the effect of various solutes on the reduction of radiation-induced defects in W alloys. Their results indicate that the segregation of Re and V at GBs enhances their sink efficiency of interstitials. Correspondingly, Liu *et al* [100] observed the segregation of Re at GBs and reduction of large interstitial clusters through their collision cascade simulations.

Zhao [101] conducted an in-depth exploration of the impact of chemical segregation on the interactions between GBs and defects in CuNiCoFe HEA. He computed the formation energies of interstitials and vacancies using three distinct models, and plotted their distributions in the vicinity of the GBs in figure 11. In the first model (average model), figures 11(a) and (d), an average interatomic interaction neglecting compositional fluctuations was applied to represent HEA's average properties. In the second model (random model), figures 11(b) and (e), solute atoms were randomly distributed introducing chemical fluctuations and lattice distortion. In the third model (segregation model), figures 11(c) and (f), strong segregation of Cu was achieved at GBs. As illustrated in figure 11, the formation energies are reduced at GBs compared to grain interior, and the reductions are more pronounced for interstitials than for vacancies. As described before, such difference indicates stronger sink efficiency for interstitials than vacancies at GBs. In contrast to the average model, the random model exhibits substantial decreases in formation energies especially for vacancies, which may result from local chemical fluctuation and lattice distortion. Intriguingly, with presence of GB segregation in the third model, the formation energies for vacancies are further reduced, while those for interstitials are elevated compared to the random model. These results suggest that the chemical heterogeneity diminishes the biased sink strengths of GBs for irradiation-induced interstitial

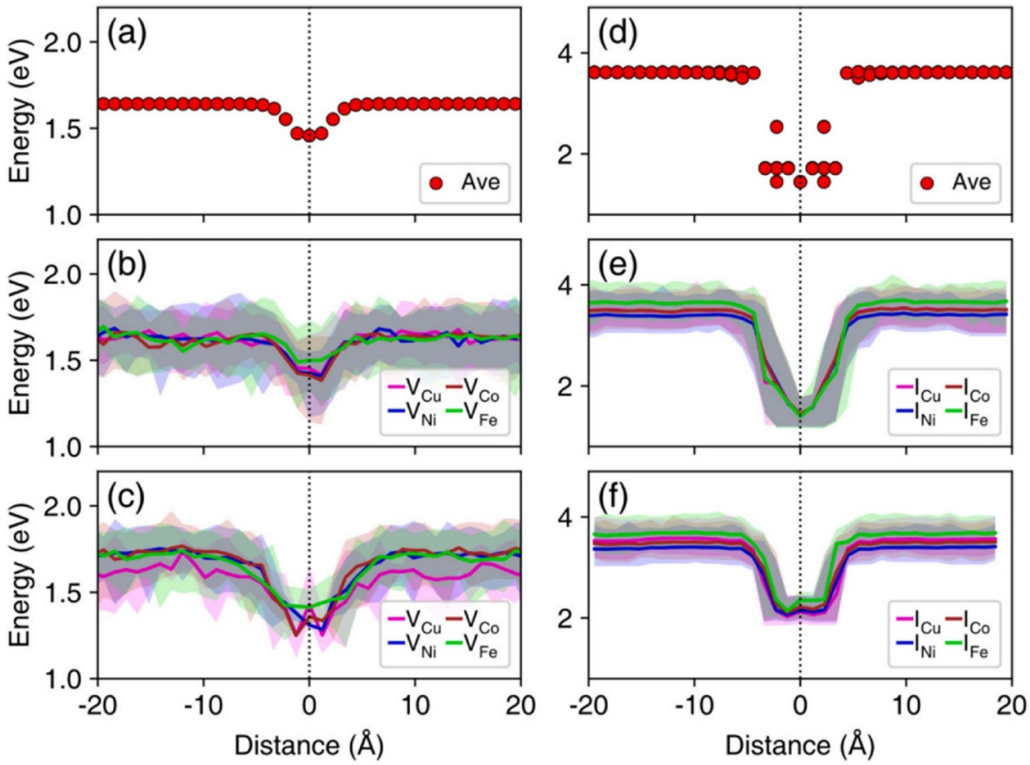

Figure 11. Distribution of formation energies of point defects near a Σ11 {113} STGB in CuNiCoFe HEA using an average model (a), (d), a random model (b), (e), and a segregation model (c), (f). The left and right columns depict the distributions of formation energies distributions of vacancies and interstitials, respectively. The shaded area represents the range of formation energies calculated from random and segregation models. Reprinted from [101], Copyright (2021), with permission from Elsevier.

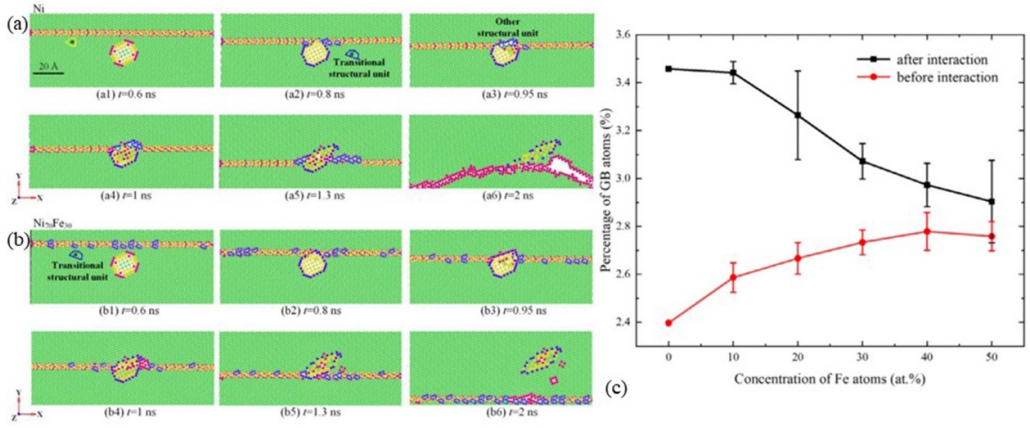

Figure 12. (a), (b) Snapshot showing the healing of SFT by GB migration in Ni (a) and $Ni_{70}Fe_{30}$ (b). Purple and yellow atoms are associated with the SFT's initial border and interior, respectively. The transitional structural units are colored blue. (c) Percentage of GB atoms before and after GB-SFT interactions, depending on the Fe concentration. Reprinted from [65], Copyright (2022), with permission from Elsevier.

and vacancies. This reduction may enhance the irradiation tolerance of HEAs, as more interstitials may be retained in the interior of grains and recombine with the vacancies.

In addition to chemical segregation, irradiation also induces migration of GBs, adding the complexity to the interactions of GBs with irradiation damage [91, 102]. Experiments have observed that the introduction of solute atoms may alter the structure of GBs [103]. This has been substantiated by Li *et al* [65] with the findings that Fe solute atoms in Ni–Fe alloys results in rougher and more disordered GBs. The LCO in GB in the $Ni_{70}Fe_{30}$ alloy leads to the emergence of transitional structural units, which are outlined in blue in figure 12(b), in contrast to pure Ni, figure 12(a). The substantial free volume of the transitional structural units enhances the GB absorption of vacancies, thereby facilitating the healing of the SFT in $Ni_{70}Fe_{30}$. The healing efficiency depending on the Fe concentration is manifested in figure 12(c). With increase of Fe concentration, the percentage of GB atoms before their interaction with the SFT increases, indicating the roughening of GB by Fe atoms, while the gap before and after the GB-SFT interaction diminishes, implying the improvement of healing capability by adding Fe concentration.

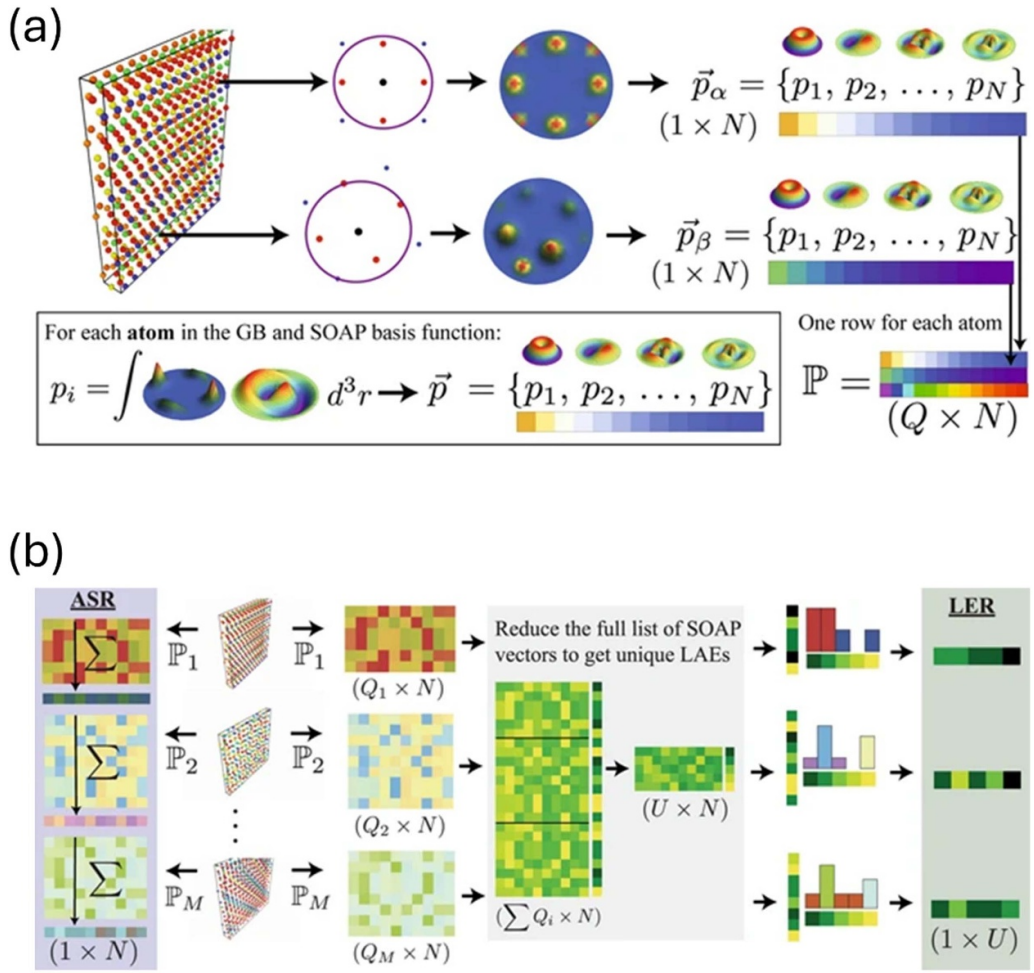

Figure 13. (a) The method for creating a SOAP matrix $\mathbb{P}$ for an individual grain boundary (GB). The help of the Gaussian density functions of single atom within a cutoff radius are calculated. And the densities are then transformed into a spectral basis that includes radial and spherical harmonics, as indicated in the highlighted area. The output from each basis function contributes to a coefficient in the vector $\vec{p}$. By compiling SOAP vectors for all atoms within the GB, a comprehensive matrix $\mathbb{P}$ is formed to represent the entire GB. (b) The calculation of ASR and LER with the SOAP matrix $\mathbb{P}$. For ASR, the summing across the columns of matrix yields an averaged SOAP vector that encapsulates the collective GB. For LER, SOAP vectors from all GBs are aggregated and refined into a set of unique vectors through similarity metrics, each representing a distinct LAE. A histogram for each GB quantifies the presence of each unique vector, creating a new vector (the LER) that reflects the fractional presence of each LAE, with components summing to 1. Reproduced from [111]. CC BY 4.0.

6. Application of machine learning in metastable GBs

While traditional methods have provided valuable insights into the behavior and characteristics of disorder systems like GBs, the complexity and huge volume of data involved in these studies are driving researchers towards data-driven techniques such as ML, which are computationally much more efficient [104]. ML achievements in recent years offer new ways to study amorphous materials or multi-element alloys which contain disorders [105–110].

Rosenbrock *et al* [111] applied ML techniques to identify and analyze the 'building blocks' of atomic systems, focusing on GBs in FCC nickel systems. They utilized the Smooth Overlap of Atomic Positions (SOAP) descriptor for characterizing local atomic environments (LAEs) around GBs and developed two feature extraction methods: the Averaged SOAP Representation (ASR) and the Local Environment Representation (LER). As is shown in figure 13(a), SOAP descriptors are used to effectively characterize the LAEs surrounding GBs. The vectors of all atoms in the GB form a matrix $\mathbb{P}$ with each row representing each atom.

Subsequently, figure 13(b) introduces the two distinct methodologies for feature extraction. The ASR compresses the SOAP vectors across all atoms within a single GB, yielding a singular descriptor that encapsulates the average LAE for the entirety of the GB. The LER, on the other hand, constructs a histogram representing the distribution of unique LAEs detected across all GBs, thereby providing a comprehensive snapshot of the atomic landscape within each boundary. Through ML models, they predicted GB properties such as energy, temperature-dependent mobility, and shear coupling. The LER approach provided insights into specific LAEs influencing GB properties, bridging high-dimensional atomic data with physical properties in an interpretable manner.

Fan *et al* [112] used regularized L2-loss support vector regression (SVR) for the study of property relationships between structural flexibility (SF) and stress-driven shear transformation. The study introduced a novel structural quantity, known as SF, to transform the static structure x_i into a quantity that is more focused on properties and easier for users to understand and apply. The SF for the atom i is:

$$\mathrm{SF}_i = \omega^T x_i,$$

where ω is the weighting vector. For the ML model, they use $y_i = \ln(v_{\mathrm{flex},i})$ as the supervisory signal and the loss function is shown as follows:

$$L = \frac{1}{2}\omega^T\omega + C\sum_{i=1}^{l}\left[\max\left(0, \left|y_i - \omega^T x_i\right| - \varepsilon\right)\right]^2.$$

Here, C is the regularization parameter and ε is the parameter related to the sensitivity. Through ML, the optimal ω was calculated. Fan *et al* also showed that there is strong correlation between SF and a variety of properties in metallic glasses, demonstrating the effectiveness in bridging local static structure with the material's dynamic responses.

In interfaces-specific scenarios, various ML techniques help researchers find out the structure-properties relationship in a new and more efficient way. Kedharnath *et al* [113] applied the eXtreme Gradient Boosting and SHapley Additive exPlanations to extract the relationship between parameters of MD and the yield stress in GBs. In another research done by Oda *et al* [114], non-linear support vector machine based on virtual screening (VS) was used to establish prediction models that can successfully predict the structures and energies of GBs. A combined density functional theory (DFT) and ML method was to investigate interfacial friction between corrugated graphene sheets by Liu *et al* [115]. In another study done by Tang *et al* [116], in order to understand the interface structure and band offset in a CdS/CdTe heterostructure, they leveraged a neural-network-based ML method combined with stochastic surface walking-based global optimization. Yang *et al* [117], in their recent work, explored several ML classification methods including ensemble methods and Bayes-based methods. Bayesian networks demonstrated superior performance in analysis of the influence of these microstructural features on twin nucleation. Fotos *et al* [118] applied convolutional neural networks to their GB research. A semantic segmentation model is trained to recognize and categorize each pixel in an image, significantly focusing on phase separation and boundary detection.

Mahmood *et al* [119] developed a Gaussian Process Regression (GPR) model aimed at delivering a probabilistic characterization of GB segregation energy. Their emphasis was on exploring the connection between GB segregation energy ΔE and the excess atomic volume $\frac{\Delta V}{V_0}$ within metastable GBs. Specifically, in this study, the relationship between the model's inputs, the excess atomic volume, denoted as x,

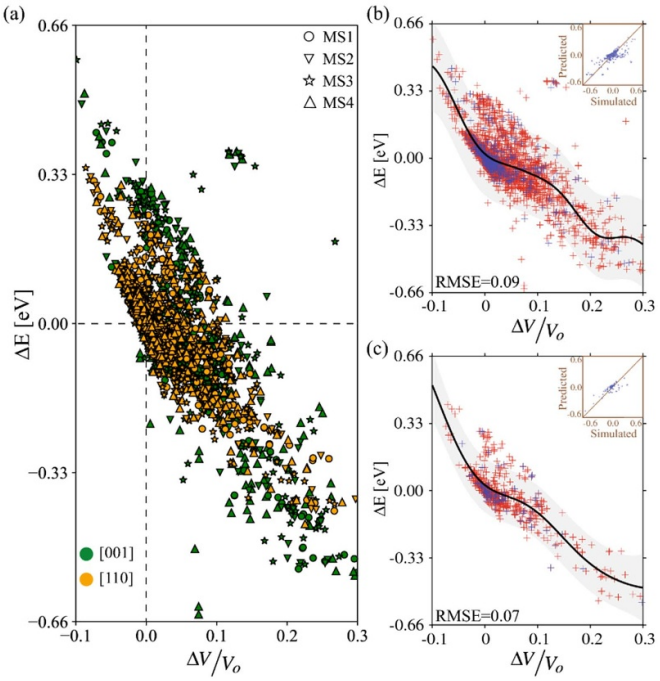

Figure 14. (a) The Gaussian Process Regression (GPR) machine learning model predicts segregation energy as a function of specific parameters. (b) The GPR model utilizes atomistic data from all metastable structures (MS1, MS2, MS3, and MS4) to predict segregation energy. (c) Similar to (b), the GPR model is applied to only the lowest GB energy structure (MS1). Reproduced from [119]. CC BY 4.0.

and its outputs y, the segregation energy, can be described by a Gaussian process, symbolized as $f(x)$:

$$y = f(x) + \varepsilon,$$

$$f(x) \sim GP\left(\mu(x), k_{SE}(x,x')\right),$$

$$\varepsilon \sim \mathcal{N}\left(0, \sigma_n^2\right),$$

$$k_{\mathrm{SE}}(x,x') = \sigma_f^2 e^{-\frac{(x-x')^2}{2l^2}},$$

where $\mu(x)$ is the mean function and $k_{\mathrm{SE}}(x,x')$ is the covariance function. σ_f and l are the GPR hyperparameters. Their research revealed that alloying elements have a significant impact on GBs, influencing microstructural evolution and transport properties. Furthermore, the study demonstrated that changes in atomic Voronoi volume resulting from GB metastability have a direct influence on segregation energy, as illustrated in figure 14.

Despite the powerfulness of these ML methods, they often operate as 'black boxes', e.g. deep neural networks, making it difficult to understand the inner physics. Most ML approaches focus on average properties or lack interpretability, missing

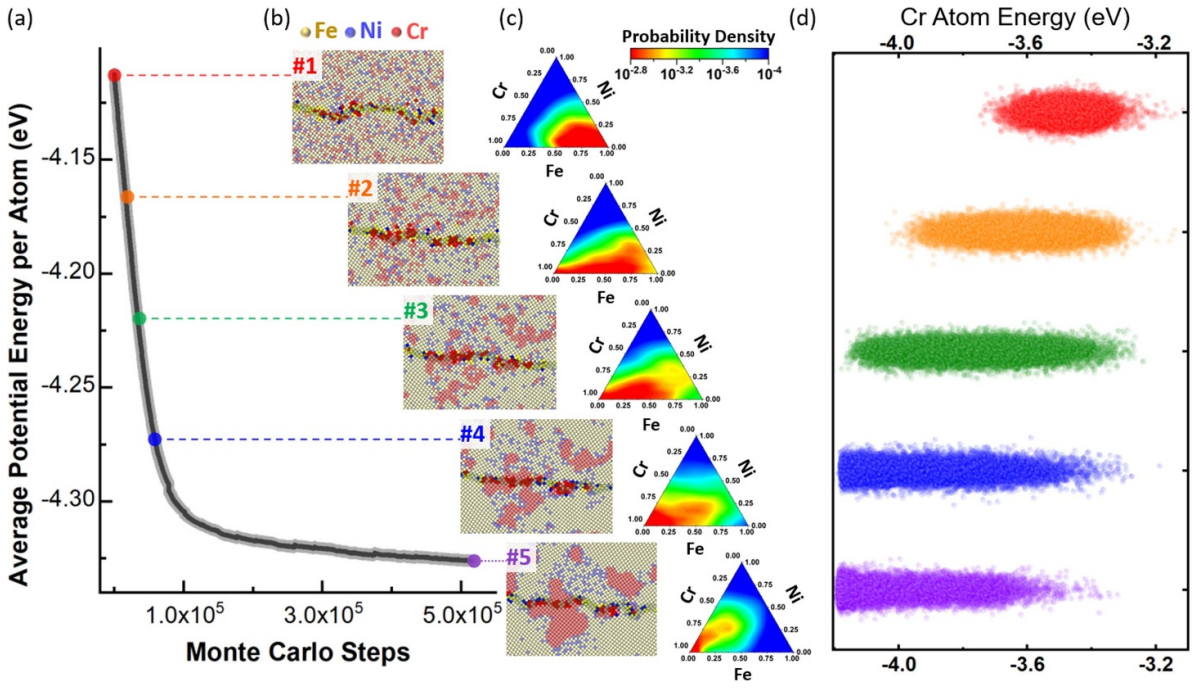

Figure 15. (a) The energetic profile and (b) structural details in a Σ25 (710) bi-crystal $Fe_{70}Ni_{10}Cr_{20}$ sample analyzed via MC metropolis algorithm. (c) Illustration of Cr atoms' surrounding chemical composition in ternary diagrams. (d) Energy variation of Cr atoms across chosen sample states. Reprinted from [123], Copyright (2021), with permission from Elsevier.

out on local details [120, 121]. As is known, the performance of the GB-involved materials is affected by the distribution of chemical elements like Cr in FeNiCr stainless steels [75, 122]. To study the effect of the chemical complexity, in another research by Wang *et al* [123], a physics-based ML approach was designed for prediction of the system's energy (E) and activation barrier (E_A) of Cr atoms near GBs under various conditions. Unlike traditional ML methods, the approach uses parameters with clear physical meanings, like local electronegativity and atomic packing. In this study, various FeNiCr samples with different chemical compositions and GB angles were established to examine the energetic and kinetic properties of Cr atoms. Specifically, they built symmetric tilt <100> GBs, employed an embedded atom method potential aligned with DFT calculations [124]. The focus was on coincident site lattice GBs under periodic boundary conditions. Initially, the samples were solid solutions with randomly placed atoms, and then a metropolis MC algorithm to find energetically more stable states accompanies with chemical heterogeneity (figures 15(a) and (b)). The simulations showed that well-segregated states of Cr are more stable than RSS. Significant variations were observed in the local chemical environments of Cr atoms and their corresponding energy, which fluctuated by over 1 eV (figure 15(d)).

In this study, the kinetic mobility of Cr atoms was assessed by examining their activation barriers, which are key to understanding atomic movements. ART technique was used to explore the PEL and determine the energy activation (E_A) spectra of Cr.

The algorithm in this study is designed within a physics-based parameter space, spanned by the local electronegativity and Voronoi volume. The local electronegativity of a specific atom i is calculated as a Gaussian-weighted average of the electronegativity of nearby atoms, denoted as χ_j:

$$\chi_i \equiv \frac{\sum_j \exp\left(-\frac{r_{ij}^2}{2\sigma^2}\right)\chi_j}{\sum_j \exp\left(-\frac{r_{ij}^2}{2\sigma^2}\right)},$$

where r_{ij} is the distance between the atom i and atom j, and σ is set as 3.0 Å. The local free volume V_v is determined by the Voronoi polyhedral volume around an atom, representing the chemical environment and physical packing [125, 126]. To avoid the 'black box', regularized ridge regression is used to find the optimal weight vector ω that minimizes the L2 loss for all Cr atoms, and also shows the importance of the features. The optimal weight vector is then applied for further testing and prediction.

$$\omega^* = \min_{\omega} ||y - X\omega||_2^2 + \lambda ||\omega||_2^2.$$

Here, y represents the vector of supervisory signals, which is the energy of the system or the activation barriers in this study, while $\boldsymbol{X}$ denotes a matrix where each row corresponds to the feature vector of the i-th atoms within the space, and the regularization parameter λ is set to be non-negative. The optimal weight vector, ω^*, derived via the ML algorithm, is subsequently applied to future testing and prediction.

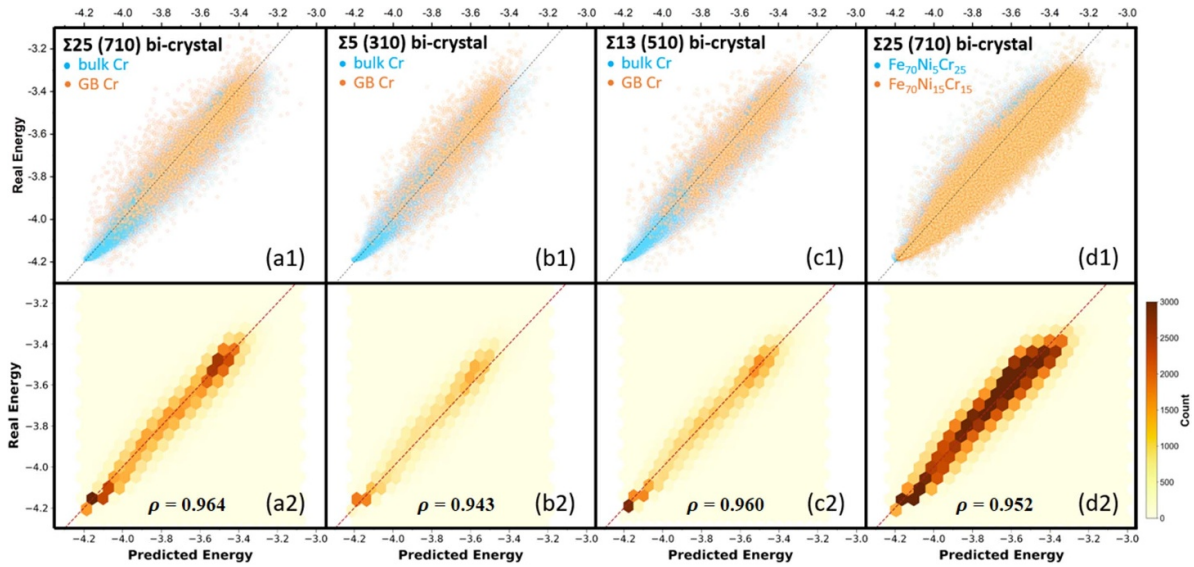

Figure 16. Contrast between ML predictions and real energy of Cr atoms, also the Pearson correlation coefficients ρ in various systems: (a) Σ25 (710) (b) Σ5 (310), (c) Σ13 (510), and (d) $Fe_{70}Ni_5Cr_{25}$ and $Fe_{70}Ni_{15}Cr_{15}$ bi-crystal systems, respectively. Reprinted from [123], Copyright (2021), with permission from Elsevier.

The ML model's ability to predict Cr atoms' energy was evaluated using a dataset derived from the Σ25 (710) GB system. This involved dividing 80 160 Cr atoms into a training set (20%) and a testing set (80%) based on MC structures. Additionally, the model's performance was tested under various compositions and GB angles without further training. As shown in figure 16(a1), predictions are closely aligned with real values across different scenarios. For instance, in the Σ25 (710) GB system, both training and testing data show good correlation between predicted and real Cr atom energy. This is visually confirmed by a density plot in figure 16(a2), where most data points align along the diagonal, indicating the model's robustness. Furthermore, the model's efficacy was demonstrated in predicting Cr atom energy in different GBs (Σ5 (310) and Σ13 (510)) and chemical compositions ($Fe_{70}Ni_5Cr_{25}$ and $Fe_{70}Ni_{15}Cr_{15}$). The testing data in these scenarios, as evidenced by high Pearson correlation coefficients ρ in figure 16, suggests the model's reliability in various chemical environments and microstructures, ranging from initially RSS to well-segregated states.

The model was then applied to predict the activation energy (E_A) spectrum of Cr atoms in GBs. And the ML model was later tested on various samples with different chemistries and GB angles. Unlike energy calculations with explicit values, for kinetics, a single atom can get involved in multiple local rearrangement events, making direct correlation plots inapplicable. Instead, contrasting activation barrier spectra between the most and least mobile atoms, as predicted by ML, proves to be more effective. Figure 17(a) illustrates real distribution of E_A in the Σ25 (710) GB sample, which are predicted to have the lowest and highest 10% of mobility. Figure 17(b) shows the predictions in a random solid-solution sample. The results from a different Σ5 (310) GB system are shown in figures 17(c) and (d), both in well-segregated and solid-solution states.

Figure 18 shows the ML-predicted system's energy and effective E_A in the space spanning by $\chi - V_v$. It is observed that smaller local Voronoi volume and electronegativity enhance Cr's thermodynamic stability, with electronegativity showing greater sensitivity. Conversely, Voronoi volume significantly influences kinetic properties. It is believed that the data in figures 18(a) and (b) can help design austenitic alloys with specific thermodynamic and kinetic characteristics, achievable through compositional and manufacturing adjustments. For example, regions marked in figure 18 indicate low energy and small activation barriers for Cr atoms, suggesting favorable thermodynamic states and enhanced diffusion. This result aligns well with Kim *et al*'s findings [122], where Cr-segregated GBs environments correlate with the presence of a protective Cr_2O_3 layer near GBs.

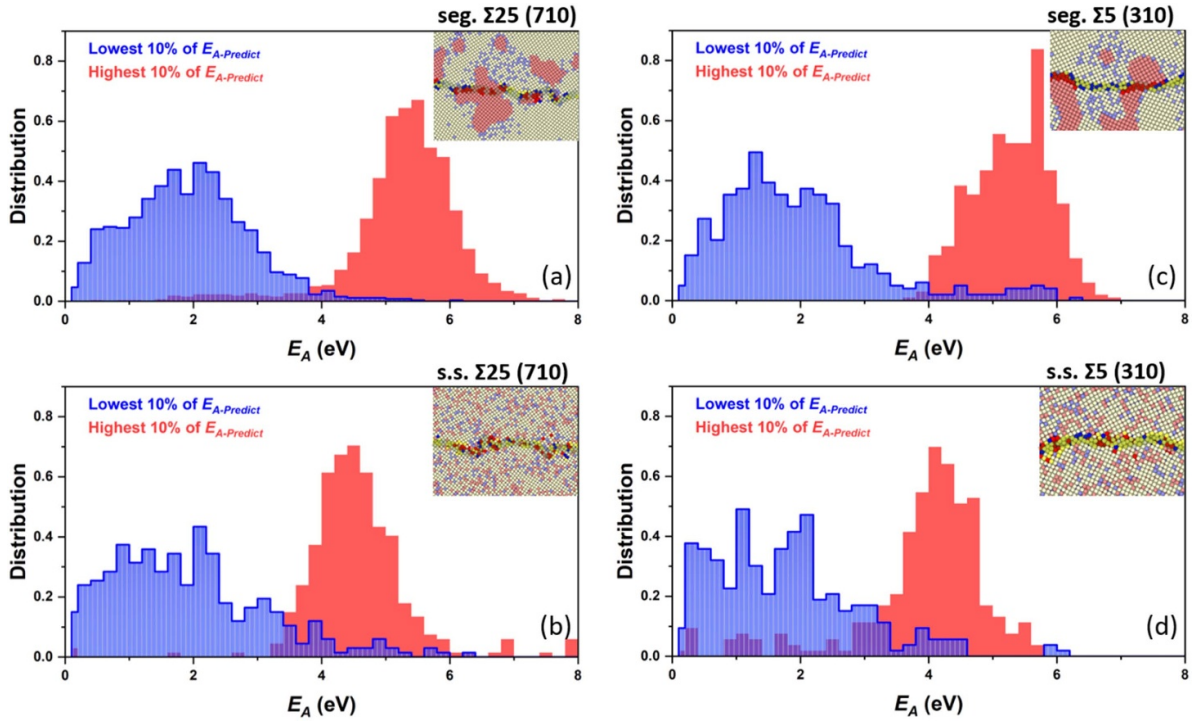

Figure 17. The distribution of E_A of the Cr atoms, categorized by the model into the lowest and highest 10% mobility, in (a) segregated Σ25 (710) (b) RSS Σ25 (710), (c) segregated Σ5 (310) system, and (d) RSS Σ5 (310) bi-crystal system, respectively. Reprinted from [123], Copyright (2021), with permission from Elsevier.

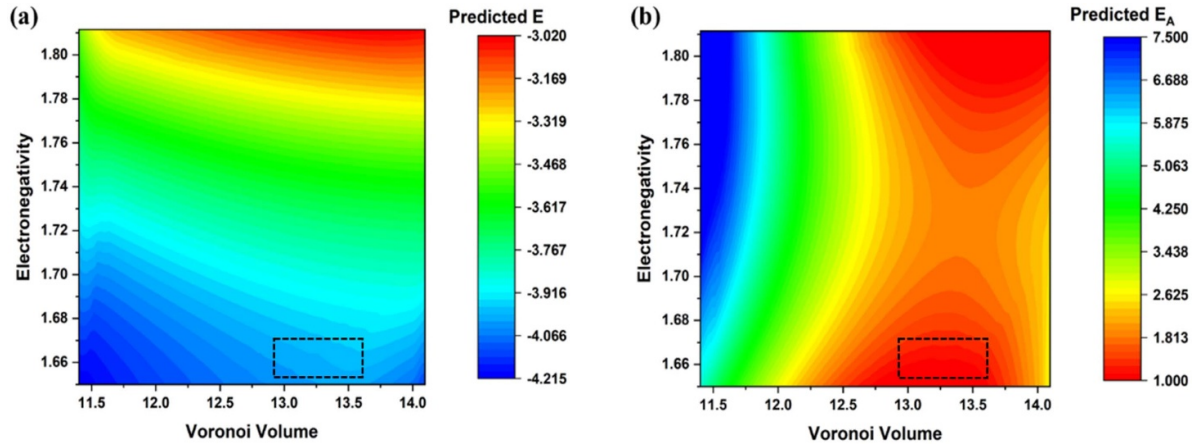

Figure 18. The predicted (a) energy E and (b) E_A of Cr atoms in the parameter space spanned by the Voronoi volume and the local electronegativity. Reproduced with permission from [123].

7. Summary and outlook

In this topical review we have briefly introduced metastable GBs' microstructures, energetics, and kinetics, as well as their non-equilibrium evolution and concomitant properties changes under external thermo-mechano-irradiation stimuli. Recent progresses have demonstrated that, even without altering samples' textures or the macroscopic misorientation angles between neighboring grains, there is plenty of space to manipulate the metastable microstates of GBs and hence to harness the performance of interface-rich materials. Below are some important findings from previous studies:

- Metastable GBs exhibit unique energetic and kinetic behaviors compared to ground-state GBs. At fixed misorientation, the energy of metastable GBs exhibits a spectrum instead of a single value, featuring a series of local minima in the systems PEL. The local minima in the PEL and the shape of interconnection pathways between them govern the kinetic evolution of GBs, which is similar to glassy materials. Through exploration of the IS energies in the PEL, computational studies have revealed the ageing/rejuvenating mechanisms and activation barrier distributions for metastable GBs. Diffusion in non-equilibrium GBs is facilitated by rough energy landscape, i.e. high fraction of pathways with

easy accessibility and low activation barriers, instead of free volume. The computational results suggest a boost in the GB diffusion in metastable GBs, which is supported by experimental observations. In addition, with low activation barrier, abnormal non-Arrhenius GB migration has been observed.

- The unique energetic and kinetic behaviors of metastable GBs impart crucial implications for the mechanical properties of nanocrystalline materials. Inverse relationships between GB energy and yield strength have been discovered by previous studies. Other studies have revealed that in addition to the energetics, the local structural disorder also affects the yield strength and GB sliding mechanism. In experiments, the metastable GBs are induced by laser irradiation. It has been found that increasing laser fluence leads to the decrease of hardness, and following annealing recovers the metastable GBs towards low-energy states and elevation of the hardness.
- Chemical complexity in multi-components alloys could also drive the GBs away from their ground states, further enriching the possible metastable microstates a GB can possess. Such a chemical complexity-induced metastability could in turn largely impact the mechanical stability and deformation mechanisms of NG HEAs and other complex multi-component systems. Simulations and experimental studies have demonstrated that the presence of chemical heterogeneity at GBs can significantly enhance their resistance to dislocation nucleation and movement, contributing to the overall strength and ductility of the material. The effect of chemical complexity is highly dependent on the element segregation at the GBs, where some elements can promote more stable and resistant GB structures under mechanical loading. Under certain extreme conditions such as irradiation, structural disorders and chemical complexity can concurrently present and interplay with each other. Previous studies have found that, depending on specific irradiation conditions, the interplay between chemical complexity and structural disorder can bring GBs towards different microstates and energetics. In turn, the segregation of certain solute atoms on GBs increases the sink effect of defects, improving the system's damage resistance.
- Given the vastness of the chemical-structural phase space for metastable GBs, ML techniques have been increasingly employed in recent years to decipher the structure-property relationship. Compared with the 'black-box' type ML techniques in early days, more physics-based, transparent, and interpretable ML algorithms have been developed recently and made significant progress. And some non-monotonic and non-intuitive thermodynamics/kinetics behaviors have been discovered by ML at the GBs in the present of both structural disorders and chemical heterogeneity.

The unique behaviors of metastable GBs, in conjunction with emerging data-driven techniques such as ML, present new GB-engineering opportunities and route, which could further expand the tunability of nano-structured materials in a predictive manner. And we hope this topical review paper could help stimulate the efforts on developing such new GBs engineering strategies.

Data availability statement

No new data were created or analysed in this study.

ORCID iD

Miao He https://orcid.org/0000-0003-1023-1040

References

[1] Mishin Y, Asta M and Li J 2010 Atomistic modeling of interfaces and their impact on microstructure and properties *Acta Mater.* **58** 1117–51
[2] Hu J, Shi Y N, Sauvage X, Sha G and Lu K 2017 Grain boundary stability governs hardening and softening in extremely fine nanograined materials *Science* **355** 1292–6
[3] Meyers M A, Mishra A and Benson D J 2006 Mechanical properties of nanocrystalline materials *Prog. Mater. Sci.* **51** 427–556
[4] Zhou Y, Yang Z and Lu Z 2014 Dynamic crack propagation in copper bicrystals grain boundary by atomistic simulation *Mater. Sci. Eng.* **599** 116–24
[5] Rupert T J and Schuh C A 2010 Sliding wear of nanocrystalline Ni-W: structural evolution and the apparent breakdown of Archard scaling *Acta Mater.* **58** 4137–48
[6] Lu L, Chen X, Huang X and Lu K 2009 Revealing the maximum strength in nanotwinned copper *Science* **323** 607–10
[7] van Swygenhoven H and Weertman J R 2006 Deformation in nanocrystalline metals *Mater. Today* **9** 24–31
[8] Schuler J D, Barr C M, Heckman N M, Copeland G, Boyce B L, Hattar K and Rupert T J 2019 In situ high-cycle fatigue reveals importance of grain boundary structure in nanocrystalline Cu-Zr *JOM* **71** 1221–32
[9] Khalajhedayati A, Pan Z and Rupert T J 2016 Manipulating the interfacial structure of nanomaterials to achieve a unique combination of strength and ductility *Nat. Commun.* **7** 10802
[10] Raabe D, Herbig M, Sandlöbes S, Li Y, Tytko D, Kuzmina M, Ponge D and Choi P-P 2014 Grain boundary segregation engineering in metallic alloys: a pathway to the design of interfaces *Curr. Opin. Solid State Mater. Sci.* **18** 253–61
[11] van Beers P R M, Kouznetsova V G, Geers M G D, Tschopp M A and McDowell D L 2015 A multiscale model of grain boundary structure and energy: from atomistics to a continuum description *Acta Mater.* **82** 513–29
[12] Olmsted D L, Foiles S M and Holm E A 2009 Survey of computed grain boundary properties in face-centered cubic metals: i. Grain boundary energy *Acta Mater.* **57** 3694–703
[13] Sutton A P and Balluffi R W 1997 Interfaces in crystalline materials *J. Solid State Electrochem.* **1** 117–8
[14] Frolov T, Olmsted D L, Asta M and Mishin Y 2013 Structural phase transformations in metallic grain boundaries *Nat. Commun.* **4** 1899
[15] Zhu Q, Samanta A, Li B, Rudd R E and Frolov T 2018 Predicting phase behavior of grain boundaries with evolutionary search and machine learning *Nat. Commun.* **9** 467
[16] Kashinath A, Misra A and Demkowicz M J 2013 Stable storage of Helium in nanoscale platelets at semicoherent interfaces *Phys. Rev. Lett.* **110** 086101
[17] Vattré A, Jourdan T, Ding H, Marinica M C and Demkowicz M J 2016 Non-random walk diffusion enhances the sink strength of semicoherent interfaces *Nat. Commun.* **7** 10424

[18] Han J, Vitek V and Srolovitz D J 2016 Grain-boundary metastability and its statistical properties *Acta Mater.* **104** 259–73

[19] Wu C, Christensen M S, Savolainen J-M, Balling P and Zhigilei L V 2015 Generation of subsurface voids and a nanocrystalline surface layer in femtosecond laser irradiation of a single-crystal Ag target *Phys. Rev.* B **91** 035413

[20] Wu C and Zhigilei L V 2016 Nanocrystalline and polyicosahedral structure of a nanospike generated on metal surface irradiated by a single femtosecond laser pulse *J. Phys. Chem.* C **120** 4438–47

[21] Kumar S, Nandi S, Pattanayek S K, Madan M, Kaushik B, Kumar R and Krishna K G 2023 Atomistic characterization of multi nano-crystal formation process in Fe-Cr-Ni alloy during directional solidification: perspective to the additive manufacturing *Mater. Chem. Phys.* **308** 128242

[22] Balbus G H, Echlin M P, Grigorian C M, Rupert T J, Pollock T M and Gianola D S 2018 Femtosecond laser rejuvenation of nanocrystalline metals *Acta Mater.* **156** 183–95

[23] Choi N *et al* 2020 Analyzing the 'non-equilibrium state' of grain boundaries in additively manufactured high-entropy CoCrFeMnNi alloy using tracer diffusion measurements *J. Alloys Compd.* **844** 155757

[24] Yokoi T, Kondo Y, Ikawa K, Nakamura A and Matsunaga K 2021 Stable and metastable structures and their energetics of asymmetric tilt grain boundaries in MgO: a simulated annealing approach *J. Mater. Sci.* **56** 3183–96

[25] Hallberg H and Blixt K H 2024 Multiplicity of grain boundary structures and related energy variations *Mater. Today Commun.* **38** 107724

[26] Homer E R, Hart G L W, Owens C B, Hensley D M, Spendlove J C and Serafin L H 2022 Examination of computed aluminum grain boundary structures and energies that span the 5D space of crystallographic character *Acta Mater.* **234** 118006

[27] Zhang H, Srolovitz D J, Douglas J F and Warren J 2009 A Grain boundaries exhibit the dynamics of glass-forming liquids *Proc. Natl Acad. Sci. USA* **106** 7735–40

[28] Debenedetti P G and Stillinger F H 2001 Supercooled liquids and the glass transition *Nature* **410** 259–67

[29] Heuer A 2008 Exploring the potential energy landscape of glass-forming systems: from inherent structures via metabasins to macroscopic transport *J. Phys.: Condens. Matter* **20** 373101

[30] Fan Y, Iwashita T and Egami T 2017 Energy landscape-driven non-equilibrium evolution of inherent structure in disordered material *Nat. Commun.* **8** 15417

[31] Zhang H and Srolovitz D J 2006 Simulation and analysis of the migration mechanism of Σ5 tilt grain boundaries in an fcc metal *Acta Mater.* **54** 623–33

[32] Barkema G T and Mousseau N 2001 *Comput. Mater. Sci.* **20** 285–92

[33] Alexander K C and Schuh C A 2013 Exploring grain boundary energy landscapes with the activation-relaxation technique *Scr. Mater.* **68** 937–40

[34] Bai Z, Balbus G H, Gianola D S and Fan Y 2020 Mapping the kinetic evolution of metastable grain boundaries under non-equilibrium processing *Acta Mater.* **200** 328–37

[35] Wei J, Feng B, Ishikawa R, Yokoi T, Matsunaga K, Shibata N and Ikuhara Y 2021 Direct imaging of atomistic grain boundary migration *Nat. Mater.* **20** 951–5

[36] Chesser I, Holm E and Runnels B 2021 Optimal transportation of grain boundaries: a forward model for predicting migration mechanisms *Acta Mater.* **210** 116823

[37] Starikov S, Abbass A, Drautz R and Mrovec M 2023 Disordering complexion transition of grain boundaries in bcc metals: insights from atomistic simulations *Acta Mater.* **261** 119399

[38] Bai Z, Misra A and Fan Y 2022 Universal trend in the dynamic relaxations of tilted metastable grain boundaries during ultrafast thermal cycle *Mater. Res. Lett.* **10** 343–51

[39] Mahjoub R, Ferry M and Stanford N 2022 Grain boundary kinetics in magnesium alloys from first principles *Comput. Mater. Sci.* **210** 111042

[40] Bean J J and McKenna K P 2016 Origin of differences in the excess volume of copper and nickel grain boundaries *Acta Mater.* **110** 246–57

[41] Suzuki A and Mishin Y 2005 Atomic mechanisms of grain boundary diffusion: low versus high temperatures *J. Mater. Sci.* **40** 3155–61

[42] Alsayed A M, Islam M F, Zhang J, Collings P J and Yodh A G 2005 Premelting at defects within bulk colloidal crystals *Science* **309** 1207–10

[43] Aidhy D S, Zhang Y and Weber W H 2014 A fast grain-growth mechanism revealed in nanocrystalline ceramic oxides *Scr. Mater.* **83** 9–12

[44] Liu C, Guan P and Fan Y 2018 Correlating defects density in metallic glasses with the distribution of inherent structures in potential energy landscape *Acta Mater.* **161** 295–301

[45] Vaidya M, Trubel S, Murty B S, Wilde G and Divinski S V 2016 Ni tracer diffusion in CoCrFeNi and CoCrFeMnNi high entropy alloys *J. Alloys Compd.* **688** 994–1001

[46] Homer E R, Johnson O K, Britton D, Patterson J E, Sevy E T and Thompson G B 2022 A classical equation that accounts for observations of non-Arrhenius and cryogenic grain boundary migration *npj Comput. Mater.* **8** 157

[47] Montes de Oca Zapiain D, Guziewski M, Coleman S P and Dingreville R 2020 Characterizing the tensile strength of metastable grain boundaries in silicon carbide using machine learning *J. Phys. Chem.* C **124** 24809–21

[48] Vo N Q, Averback R S, Bellon P and Caro A 2009 Yield strength in nanocrystalline Cu during high strain rate deformation *Scr. Mater.* **61** 76–79

[49] Vo N Q, Schäfer J, Averback R S, Able K, Ashkenazy Y and Bellon P 2011 Reaching theoretical strengths in nanocrystalline Cu by grain boundary doping *Scr. Mater.* **65** 660–3

[50] Rupert T J and Schuh C A 2011 Mechanically driven grain boundary relaxation: a mechanism for cyclic hardening in nanocrystalline Ni *Phil. Mag. Lett.* **92** 20–28

[51] Utt D, Stukowski A and Able K 2020 Grain boundary structure and mobility in high-entropy alloys: a comparative molecular dynamics study on a Σ11 symmetrical tilt grain boundary in face-centered cubic CuNiCoFe *Acta Mater.* **186** 11–19

[52] Helfferich J, Lyubimov I, Reid D and de Pablo J J 2016 Inherent structure energy is a good indicator of molecular mobility in glasses *Soft Matter* **12** 5898–904

[53] Reid D R, Lyubimov I, Ediger M D and de Pablo J J 2016 Age and structure of a model vapour-deposited glass *Nat. Commun.* **7** 13062

[54] Zhang S, Liu C, Fan Y, Yang Y and Guan P 2020 Soft-mode parameter as an indicator for the activation energy spectra in metallic glass *J. Phys. Chem. Lett.* **11** 2781–7

[55] Burbery N J, Das R and Ferguson W G 2016 Transitional grain boundary structures and the influence on thermal, mechanical and energy properties from molecular dynamics simulations *Acta Mater.* **108** 355–66

[56] Zhang L, Lu C and Shibuta Y 2018 Shear response of grain boundaries with metastable structures by molecular dynamics simulations *Modelling Simul. Mater. Sci. Eng.* **26** 035008

[57] Li Q-J, Sheng H and Ma E 2019 Strengthening in multi-principal element alloys with local-chemical-order roughened dislocation pathways *Nat. Commun.* **10** 3563

[58] Ma E 2020 Unusual dislocation behavior in high-entropy alloys *Scr. Mater.* **181** 127–33

[59] Cao F-H, Wang Y-J and Dai L-H 2020 Novel atomic-scale mechanism of incipient plasticity in a chemically complex CrCoNi medium-entropy alloy associated with inhomogeneity in local chemical environment *Acta Mater.* **194** 283–94

[60] Wu H-H, Dong L-S, Wang S-Z, Wu G-L, Gao J-H, Yang X-S, Zhou X-Y and Mao X-P 2023 Local chemical ordering coordinated thermal stability of nanograined high-entropy alloys *Rare Met.* **42** 1645–55

[61] Li X-T, Tang X-Z, Guo Y-F, Li H and Fan Y 2023 Modulating grain boundary-mediated plasticity of high-entropy alloys via chemo-mechanical coupling *Acta Mater.* **258** 119228

[62] Mousseau N, Béland L K, Brommer P, Joly J F, El-Mellouhi F, Machado-Charry E, Marinica M-C and Pochet P 2012 The activation-relaxation technique: art nouveau and kinetic art *J. At. Mol. Phys.* **2012** 925278

[63] Fan Y, Iwashita T and Egami T 2014 How thermally activated deformation starts in metallic glass *Nat. Commun.* **5** 5083

[64] Cancès E, Legoll F, Marinica M C, Minoukadeh K and Willaime F 2009 Some improvements of the activation-relaxation technique method for finding transition pathways on potential energy surfaces *J. Chem. Phys.* **130** 114711

[65] Li J, Yang X, Wang P and An Q 2022 Healing stacking fault tetrahedron in NiFe solid solution alloys through grain boundary migration *J. Nucl. Mater.* **565** 153738

[66] Wang Y, Ghaffari B, Taylor C, Lekakh S, Engler-Pinto C, Godlewski L, Huo Y, Li M and Fan Y 2023 Nonmonotonic effect of chemical heterogeneity on interfacial crack growth at high-angle grain boundaries in Fe-Ni-Cr alloys *Phys. Rev. Mater.* **7** 073606

[67] Thielen M, Schaefer F, Gruenewald P, Laub M, Marx M, Meixner M, Klaus M and Motz C 2019 In situ synchrotron stress mappings to characterize overload effects in fatigue crack growth *Int. J. Fatigue* **121** 155–62

[68] Hanson J P, Bagri A, Lind J, Kenesei P, Suter R M, Gradečak S and Demkowicz M J 2018 Crystallographic character of grain boundaries resistant to hydrogen-assisted fracture in Ni-base alloy 725 *Nat. Commun.* **9** 3386

[69] Duscher G, Chisholm M F, Alber U and Rühle M 2004 Bismuth-induced embrittlement of copper grain boundaries *Nat. Mater.* **3** 621–6

[70] Sun D-S, Yamane T and Hirao K 1991 Intermediate-temperature brittleness of a ferritic 17Cr stainless steel *J. Mater. Sci.* **26** 689–94

[71] Trelles E G, Eckmann S and Schweizer C 2022 Experimental characterization of the short crack growth behavior of a ductile cast iron (DCI GJS-500) affected by intergranular embrittlement at temperatures nearby 400 °C *Int. J. Fatigue* **155** 106573

[72] Zheng L, Chellali R, Schlesiger R, Baither D and Schmitz G 2011 Intermediate temperature embrittlement in high-purity Ni and binary Ni (Bi) alloy *Scr. Mater.* **65** 428–31

[73] Jang M J, Praveen S, Sung H J, Bae J W, Moon J and Kim H S 2018 High-temperature tensile deformation behavior of hot rolled CrMnFeCoNi high-entropy alloy *J. Alloys Compd.* **730** 242–8

[74] Ming K, Li L, Li Z, Bi X and Wang J 2019 Grain boundary decohesion by nanoclustering Ni and Cr separately in CrMnFeCoNi high-entropy alloys *Sci. Adv.* **5** eaay0639

[75] Li H, Xia S, Liu W, Liu T and Zhou B 2013 Atomic scale study of grain boundary segregation before carbide nucleation in Ni–Cr–Fe Alloys *J. Nucl. Mater.* **439** 57–64

[76] Zhou X, Yu X-X, Kaub T, Martens R L and Thompson G B 2016 Grain boundary specific segregation in nanocrystalline Fe (Cr) *Sci. Rep.* **6** 34642

[77] Lin Z, Leveugle E, Bringa E M and Zhigilei L V 2010 Molecular dynamics simulation of laser melting of nanocrystalline Au *J. Phys. Chem.* C **114** 5686–99

[78] Levo E, Granberg F, Fridlund C, Nordlund K and Djurabekova F 2017 Radiation damage buildup and dislocation evolution in Ni and equiatomic multicomponent Ni-based alloys *J. Nucl. Mater.* **490** 323–32

[79] Zhang X *et al* 2018 Radiation damage in nanostructured materials *Prog. Mater. Sci.* **96** 217–321

[80] El-Atwani O, Esquivel E, Aydogan E, Martinez E, Baldwin J K, Li M, Uberuaga B P and Maloy S A 2019 Unprecedented irradiation resistance of nanocrystalline tungsten with equiaxed nanocrystalline grains to dislocation loop accumulation *Acta Mater.* **165** 118–28

[81] Xiao X, Chu H and Duan H 2016 Effect of grain boundary on the mechanical behaviors of irradiated metals: a review *Sci. China Phys. Mech. Astron.* **59** 664601

[82] Zhang Y *et al* 2019 Thermal stability and irradiation response of nanocrystalline CoCrCuFeNi high-entropy alloy *Nanotechnology* **30** 294004

[83] Nagase T, Rack P D, Noh J H and Egami T 2015 *In-situ* TEM observation of structural changes in nano-crystalline CoCrCuFeNi multicomponent high-entropy alloy (HEA) under fast electron irradiation by high voltage electron microscopy (HVEM) *Intermetallics* **59** 32–42

[84] Levo E, Granberg F, Utt D, Able K, Nordlund K and Djurabekova F 2019 Radiation stability of nanocrystalline single-phase multicomponent alloys *J. Mater. Res.* **34** 854–66

[85] Chimi Y, Iwase A, Ishikawa N, Kobiyama M, Inami T and Okuda S 2001 Accumulation and recovery of defects in ion-irradiated nanocrystalline gold *J. Nucl. Mater.* **297** 355–7

[86] Han W Z, Demkowicz M J, Fu E G, Wang Y Q and Misra A 2012 Effect of grain boundary character on sink efficiency *Acta Mater.* **60** 6341–51

[87] Bai X-M, Voter A F, Hoagland R G, Nastasi M and Uberuaga B P 2010 Efficient annealing of radiation damage near grain boundaries via interstitial emission *Science* **327** 1631–4

[88] Uberuaga B P, Vernon L J, Martinez E and Voter A F 2015 The relationship between grain boundary structure, defect mobility and grain boundary sink efficiency *Sci. Rep.* **5** 9095

[89] Tschopp M A, Solanki K N, Gao F, Sun X, Khaleel M A and Horstemeyer M F 2012 Probing grain boundary sink strength at the nanoscale: energetics and length scales of vacancy and interstitial absorption by grain boundaries in α-Fe *Phys. Rev.* B **85** 064108

[90] Sakaguchi N, Watanabe S and Takahashi H 2001 Heterogeneous dislocation formation and solute redistribution near grain boundaries in austenitic stainless steel under electron irradiation *Acta Mater.* **49** 1129–37

[91] Barr C M, El-Atwani O, Kaoumi D and Hattar K 2019 Interplay between grain boundaries and radiation damage *JOM* **71** 1233–44

[92] Peng J, Cui S, Tian Y, Fang Q, Li J and Liaw P K 2022 Effects of grain boundary on irradiation-induced zero-dimensional defects in an irradiated copper *Appl. Math. Mech.* **43** 233–46

[93] Vetterick G A, Gruber J, Suri P K, Baldwin J K, Kirk M A, Baldo P, Wang Y Q, Misra A, Tucker G J and Taheri M L 2017 Achieving radiation tolerance through non-equilibrium grain boundary structures *Sci. Rep.* **7** 12275

[94] Farkas D 2020 Grain boundary structure in high-entropy alloys *J. Mater. Sci.* **55** 9173–83

[95] Baruffi C and Curtin W A 2022 Theory of spontaneous grain boundary roughening in high entropy alloys *Acta Mater.* **234** 118011

[96] Tschopp M A, Spearot D E and McDowell D L 2008 Influence of grain boundary structure on dislocation nucleation in FCC metals *Dislocations Solids* **14** 43–139

[97] Zhang J, He H, Liu W, Kang L, Yun D and Chen P 2020 Effects of grain boundaries on the radiation-induced defects evolution in BCC Fe-Cr alloy: a molecular dynamics study *Nucl. Mater. Eng.* **22** 100726

[98] Beyerlein I J, Caro A, Demkowicz M J, Mara N A, Misra A and Uberuaga B P 2013 Radiation damage tolerant nanomaterials *Mater. Today* **16** 443–9

[99] Li X-T, Tang X-Z and Guo Y-F 2023 Grain boundary-mediated reduction of radiation defects in different W-based alloys *Met. Mater. Int.* **29** 2648–59

[100] Liu L, Chen Y, Gao N, Liu Z, Gao F, Hu W and Deng H 2022 Molecular dynamics simulations of displacement cascades in tungsten and tungsten-rhenium alloys: effects of grain boundary and/or σ phase *J. Nucl. Mater.* **561** 153543

[101] Zhao S 2021 Effects of local elemental ordering on defect-grain boundary interactions in high-entropy alloys *J. Alloys Compd.* **887** 161314

[102] Wang X Y, Gao N, Xu B, Wang Y N, Shu G G, Li C L and Liu W 2018 Effect of irradiation and irradiation defects on the mobility of Σ5 symmetric tilt grain boundaries in iron: an atomistic study *J. Nucl. Mater.* **510** 568–74

[103] Ebrahimi F and Li H 2006 Grain growth in electrodeposited nanocrystalline fcc Ni-Fe alloys *Scr. Mater.* **55** 263–6

[104] Artrith N 2019 Machine learning for the modeling of interfaces in energy storage and conversion materials *J. Phys. Energy* **1** 032002

[105] Cubuk E D, Schoenholz S S, Rieser J M, Malone B D, Rottler J, Durian D J, Kaxiras E and Liu A J 2015 Identifying structural flow defects in disordered solids using machine-learning methods *Phys. Rev. Lett.* **114** 108001

[106] Liu Z, Zhou Q, Liang X, Wang X, Li G, Vanmeensel K and Xie J 2023 Alloy design for laser powder bed fusion additive manufacturing: a critical review *Int. J. Extrem. Manuf.* **6** 022002

[107] Liu C, Wang Y, Wang Y, Islam M, Hwang J, Wang Y and Fan Y 2023 Concurrent prediction of metallic glasses global energy and internal structural heterogeneity by interpretable machine learning *Acta Mater.* **259** 119281

[108] Tian L, Fan Y, Li L and Mousseau N 2020 Identifying flow defects in amorphous alloys using machine learning outlier detection methods *Scr. Mater.* **186** 185–9

[109] Zhou Z, Zhou Y, He Q, Ding Z, Li F and Yang Y 2019 Machine learning guided appraisal and exploration of phase design for high entropy alloys *npj Comput. Mater.* **5** 128

[110] Ward L, O'Keeffe S C, Stevick J, Jelbert G R, Aykol M and Wolverton C 2018 A machine learning approach for engineering bulk metallic glass alloys *Acta Mater.* **159** 102–11

[111] Rosenbrock C W, Homer E R, Csányi G and Hart G L 2017 Discovering the building blocks of atomic systems using machine learning: application to grain boundaries *npj Comput. Mater.* **3** 29

[112] Fan Z, Ding J and Ma E 2020 Machine learning bridges local static structure with multiple properties in metallic glasses *Mater. Today* **40** 48–62

[113] Kedharnath A, Kapoor R and Sarkar A 2024 Dislocation–grain boundary interactions in Ta: numerical, molecular dynamics, and machine learning approaches *J. Mater. Sci.* **59** 243–57

[114] Oda H, Kiyohara S and Mizoguchi T 2019 Machine learning for structure determination and investigating the structure-property relationships of interfaces *J. Phys. Mater.* **2** 034005

[115] Liu Z, Zhao X, Wang H, Ma Y, Gao L, Huang H, Yan Y, Su Y and Qiao L 2021 A first-principles and machine learning combined method to investigate the interfacial friction between corrugated graphene *Modelling Simul. Mater. Sci. Eng.* **29** 035011

[116] Tang Q, Yang J H, Liu Z P and Gong X G 2020 Directly determining the interface structure and band offset of a large-lattice-mismatched CdS/CdTe heterostructure *Chin. Phys. Lett.* **37** 096802

[117] Yang B, Vassilev-Galindo V and Llorca J 2024 Application of machine learning to assess the influence of microstructure on twin nucleation in Mg alloys *npj Comput. Mater.* **10** 26

[118] Fotos G, Campbell A, Murray P and Yakushina E 2023 Deep learning enhanced Watershed for microstructural analysis using a boundary class semantic segmentation *J. Mater. Sci.* **58** 14390–410

[119] Mahmood Y, Alghalayini M, Martinez E, Paredis C J J and Abdeljawad F 2022 Atomistic and machine learning studies of solute segregation in metastable grain boundaries *Sci. Rep.* **12** 6673

[120] Carvalho D V, Pereira E M and Cardoso J S 2019 Machine learning interpretability: a survey on methods and metrics *Electronics* **8** 832

[121] Oviedo F, Ferres J L, Buonassisi T and Butler K T 2022 Interpretable and explainable machine learning for materials science and chemistry *Acc. Mater. Res.* **3** 597–607

[122] Kim J-H, Kim B K, Kim D-I, Choi P-P, Raabe D and Yi K-W 2015 The role of grain boundaries in the initial oxidation behavior of austenitic stainless steel containing alloyed Cu at 700 C for advanced thermal power plant applications *Corros. Sci.* **96** 52–66

[123] Wang Y, Ghaffari B, Taylor C, Lekakh S, Li M and Fan Y 2021 Predicting the energetics and kinetics of Cr atoms in Fe-Ni-Cr alloys via physics-based machine learning *Scr. Mater.* **205** 114177

[124] Bonny G, Castin N and Terentyev D 2013 Interatomic potential for studying ageing under irradiation in stainless steels: the FeNiCr model alloy *Modelling Simul. Mater. Sci. Eng.* **21** 085004

[125] Żydek A, Wermiński M and Trybula M E 2021 Description of grain boundary structure and topology in nanocrystalline aluminum using Voronoi analysis and order parameter *Comput. Mater. Sci.* **197** 110660

[126] Sheng H W, Luo W K, Alamgir F M, Bai J M and Ma E 2006 Atomic packing and short-to-medium-range order in metallic glasses *Nature* **439** 419–25